https://doi.org/10.5194/egusphere-2026-4489
Preprint. Discussion started: 13 August 2026

Rapid simulation of 2-D contrail cross sections through Contrail Layer Approximation using Multi-crystal Particles (CLAMP) v1.0

Sebastian D. Eastham[1,2], Hamid R. Abbasi[1,2], Marc E. J. Stettler[3], Tristan Abbott[4], Zebediah Engberg[4]

[1]Brahmal Vasudevan Institute for Sustainable Aviation, Imperial College London, London, SW7 2AZ, United Kingdom
[2]Department of Aeronautics, Imperial College London, London, SW7 2AZ, United Kingdom
[3]Department of Civil and Environmental Engineering, Imperial College London, London, SW7 2AZ, United Kingdom
[4]Contrails.org, Kirkland, WA, United States of America

Correspondence to: Sebastian D. Eastham (s.eastham@imperial.ac.uk)

Abstract. Aircraft condensation trails (contrails) are increasingly studied with the aim of understanding and mitigating their climate impacts. Forming at the scale of a single aircraft, an individual contrail can take several hours to become large enough to be resolved by global-scale climate models, if they are resolved at all. High-fidelity simulations of individual contrails are too computationally intensive for use in global applications, but comparisons with existing reduced-order parameterizations have shown the need for approaches which can capture the development of size-resolved structures in the contrail as well as the dynamic interaction of contrail ice with the ambient humidity field. We introduce a new model of contrail physics, the Contrail Layer Approximation using Multi-crystal Particles (CLAMP) v1.0. CLAMP resolves challenges observed in other reduced-order models including lack of thermodynamic consistency and the inability to represent heterogeneity between the primary and secondary wakes due to gravitational sorting, providing an intermediate-fidelity simulation of a contrail with typical run times of about 60 seconds on one computational core for a 12-hour case. We use CLAMP to simulate the physics and radiative forcing of contrails across a broad parameter space, evaluating the effect of synoptic-scale downdrafts, mixing, settling, and gravity waves on contrail lifetime and climate impacts. We find that gravity wave forcing in particular may shorten contrail lifetimes, but that the stochastic nature of these effects is unlikely to be well captured by simple parameterizations. We also compare CLAMP to published results from other, more computationally expensive models, finding that it reproduces key trends in contrail properties with respect to common meteorological and aircraft parameters at a fraction of the computational cost. Furthermore, we show that carefully enforcing closed mass and energy budgets – not currently the case for most Lagrangian contrail models - can drive large differences in contrail properties, implying a potential shortcoming of current-generation contrail simulations. Although more work is needed to evaluate models against observations of real-world contrail behavior, including determining the importance of such inconsistencies, CLAMP is proposed as an alternative to existing single-contrail models for standalone contrail studies with sufficient speed and flexibility to inform emulations for use in global climate modeling applications.

https://doi.org/10.5194/egusphere-2026-4489
Preprint. Discussion started: 13 August 2026

1 Introduction

Condensation trails (contrails) are thought to be responsible for approximately half of aviation's overall contribution to climate change, comparable to the contribution from all aviation CO_2 emitted to date (Lee et al., 2021). There remains scientific uncertainty regarding the magnitude of contrail climate impacts, including the effect of using different climate modeling techniques, the role of fast cloud responses and climate feedbacks, and the challenge of establishing an equivalency between contrail and CO_2 climate responses (Bickel et al., 2020; Grobler et al., 2019; Verma and Burkhardt, 2022). Nevertheless, analyses considering multiple different climate metrics and the currently understood range of uncertainty have concluded that these impacts are sufficiently large to warrant investigation of mitigation techniques, including modifying aircraft routes to minimize formation and targeted use of sustainable aviation fuels which may result in optically thinner contrails (Borella et al., 2024; Teoh et al., 2022b).

Such proposals rely on accurate models of both meteorology and contrail physics. Inaccuracy in predictions of relative humidity makes it difficult to predict which regions must be avoided to minimize contrail formation and constrains the accuracy of guidance regarding the benefit of avoiding specific areas. However, as long as the statistics of the meteorological model (e.g. frequency, extent, and lifetime of ice supersaturated regions) are correct, the overall potential benefit of strategies for contrail impact mitigation can still be accurately assessed. This is not true when considering inaccuracy in models of contrail physics. If contrail models incorrectly represent the relationship between input parameters (e.g. meteorological conditions or aircraft parameters) and the eventual climate impact, then recommendations for contrail impact mitigation may be systematically wrong.

Accurate models are also needed to correctly interpret observations. Satellite observations are limited by the difficulty of identifying and quantifying contrail cirrus, and instead mostly capture linear contrails which contribute a relatively small fraction of the overall climate impact attributed to aircraft-induced cloudiness (Bock and Burkhardt, 2016; Chen and Gettelman, 2013; Kärcher, 2018). Continuous observations of contrails from geostationary satellites also struggle to identify newly-formed contrails (Driver et al., 2025; Euchenhofer et al., 2025), making attribution of contrails to individual flights more challenging (Geraedts et al., 2024). Models of contrail physics can fill this gap, but again this relies on those models representing the processes which dominate the evolution of observable parameters sufficiently accurately.

These models also need to be computationally efficient. Individual contrails have been observed as lasting up to 24 hours, and reaching widths up to 40 kilometers (Schumann et al., 2017). Although large eddy simulations have been used to simulate contrails at these scales (Lewellen et al., 2014; Unterstrasser and Gierens, 2010a), these are computationally intensive and infeasible for global- or even regional-scale simulations of contrail evolution. Given that an estimated 3 billion

https://doi.org/10.5194/egusphere-2026-4489
Preprint. Discussion started: 13 August 2026

kilometers of persistent contrail were formed in 2019 (Teoh et al., 2024a), modeling approaches are needed which can compromise between accuracy and speed.

1.1 Current approaches to contrail modeling at scale

One solution is to simulate individual contrail segments as Lagrangian objects, tracking the movement of the contrail centroid through the atmosphere and using meteorological data as boundary conditions. This is the approach used by the Contrail Cirrus Prediction (CoCiP) model (Schumann, 2012). CoCiP simulates each contrail segment as a 2-D Gaussian plume, parameterizing effects such as wind shear, settling, and diffusion in terms of changes in a handful of prognostic variables such as the Gaussian's altitude, major and minor axis radii, and crystal radius. This results in a model that can simulate a contrail's evolution on one computational core in a fraction of a second. However, the fundamental assumptions of CoCiP may cause it to incorrectly represent long-lived contrails. CoCiP assumes that settling or advection of the contrail centroid into air which is subsaturated will immediately result in mixing of that air throughout the contrail. Meanwhile the choice of a monodisperse size distribution, combined with the lack of information regarding the distribution of sizes within the contrail, means that phenomena such as gravitational size sorting of ice crystals are not represented. These limitations may explain why comparisons against higher fidelity models such as the Aircraft Plume Chemistry, Emissions, and Microphysics Model (APCEMM) (Fritz et al., 2020) using synthetic meteorological data have shown not only an average 3.8 times difference in lifetime-integrated optical depth (a proxy for climate impact), but also conflicting results from the two models when considering whether an increase in ambient relative humidity would increase or decrease that impact (Akhtar Martínez et al., 2025). Comparisons using more realistic meteorological conditions have not yet been performed, but the results shown indicate consistent differences in the modelled behavior throughout the contrail's lifetime.

A further disadvantage of Lagrangian approaches is the lack of thermodynamic consistency. The most common approach, used in the pyContrails implementation of CoCiP (DOI: 10.5281/zenodo.17944440), is to treat a contrail as an air mass which moves (advects) with the surrounding air. The air which "mixes in" to the contrail as it moves and settles is assumed to have a specific humidity interpolated from a meteorological forecast or reanalysis. Similarly, the entire contrail's temperature is assumed to evolve based on the interpolated path through the same reanalysis field.

This approach has two issues. First, advection of a point mass using data from an Eulerian meteorological model can result in non-physical variations in the conditions perceived by the Lagrangian model. Unless the sub-grid distributions of temperature and water vapor are known and perfectly represented in the Eulerian model's output, the time series of conditions for an advecting air mass will not necessarily conserve energy or water vapor. This is illustrated in Figure 1, which shows how the motion of a single, supersaturated (relative humidity of 110%) air mass can be appropriately represented in an Eulerian model and yet result in a Lagrangian representation which drops from 110% to 56% saturation. Even though a contrail moving with this marginally-saturated air mass should be able to persist, a Lagrangian model which

https://doi.org/10.5194/egusphere-2026-4489
Preprint. Discussion started: 13 August 2026

adopts the temperature of its "host" cell would incorrectly simulate warming and cooling of the contrail airmass while also simulating a 54% swing in the relative humidity of air being mixed into the contrail, resulting in sublimation. Although this demonstration uses a simple first-order upwind advection scheme, the same issue would apply even with perfectly accurate Eulerian transport due to the discretization error inherent to any approach relying on a fixed spatial grid. Such discretization error may provide an alternative reason to meteorological data inaccuracy in explaining why observed contrails often appear to persist within subsaturated regions (Low et al., 2025).

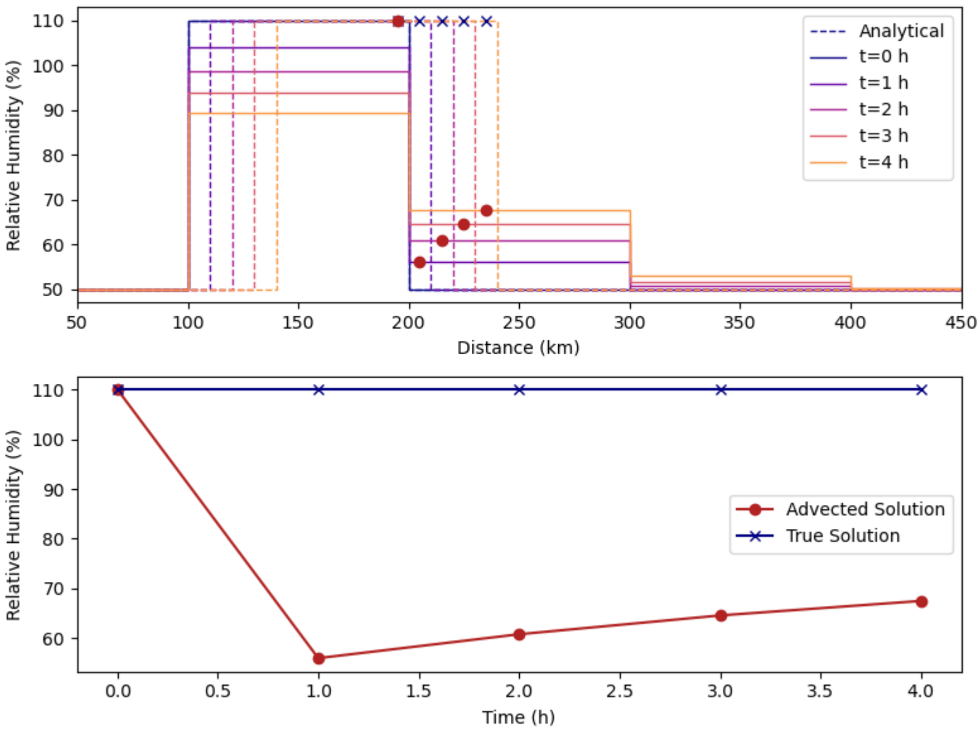

Figure 1. Demonstration of the inconsistency resulting from using an Eulerian simulation to provide boundary conditions without sufficient sub-grid information. The upper panel shows advection of a square wave from left to right at 10 km h^{-1} in a 1D domain. Advection is simulated using a simple upwind forward Euler approach, a time step of 1 hour, and a grid spacing of 100 km. Dashed lines show the analytical solution while solid lines show the result of the forward Euler advection. Crosses show the location and local relative humidity experienced by an embedded contrail, while circles show the conditions which that air mass would experience if drawing from the Eulerian simulation.

This points to the second issue, which is that allowing the ambient temperature and humidity of the contrail to change due to advection implies an "open" budget of mass and energy without any guarantee that either is conserved. While settling of the contrail ice crystals will allow them to reach "fresh" air, advection of the contrail ice with the surrounding air should not result in any change in local water mixing ratio unless mixing occurs. If this mixing is assumed to take place instantaneously into the contrail core, simulated contrail ice can be too rapidly exposed to dry air. Similarly, temperature changes should not occur without some energy input – for example, adiabatic compression due to a downdraft. A Lagrangian representation of a

https://doi.org/10.5194/egusphere-2026-4489
Preprint. Discussion started: 13 August 2026

contrail should ideally have a closed energy budget, with temperature changes driven by explicitly-resolved sources of adiabatic and diabatic heating. Models which interpolate the local temperature from an Eulerian grid as the contrail moves instead have an open energy budget, in which energy transfer becomes implicit and can be the result of grid-scale changes in temperature due to (for example) mixing of air masses. While this is not a problem when considering the behavior of air at the scale of Eulerian grid cells (typically 20-50 km for modern meteorological reanalyses), the result when following Lagrangian trajectories through a field derived from an Eulerian model is a non-physical change in boundary conditions as shown in the lower panel of Figure 1.

An approach which aims to resolve these challenges is to represent contrails as a marginal increase in cloud fraction within a global climate model (GCM). This not only ensures a closed thermodynamic budget, it also allows phenomena such as cloud feedbacks to be captured which may change the magnitude or even sign of contrail climate impacts (Bickel et al., 2020, 2025). However, GCM-based modeling of contrails relies on simplifying assumptions regarding the early evolution of the contrail. Given that GCM grid cells are typically 50-100 km in width and 500-1000 m in vertical extent, even a 12-hour-old contrail in a deep supersaturation layer experiencing sustained wind shear would take up only a fraction of a cell's volume. Since GCMs are representing a chaotic system, this also means that GCM simulations of contrail impacts often need to scale up global contrail coverage (Bickel et al., 2025) or take the average of a large ensemble of simulations (Burkhardt et al., 2018) in order to achieve a sufficient signal-to-noise ratio. These limitations not only raise the question of impact linearity, but also make GCM models less useful for investigations of the behavior of individual contrails with regards to specific interventions or evaluations against observations.

1.2 Comparison of prior work on contrail impacts and mitigation efficacy

Despite these shortcomings Lagrangian models, GCMs, and satellite-based methods are routinely used to estimate the total climate impact of contrails. An analysis by Lee et al. (2021) estimated the literature spread in calculations of contrail radiative forcing, finding that the 2018 net effective radiative forcing from aviation contrail cirrus was 57.4 mW/m^2 (90% confidence range 17 to 98 mW/m^2) compared to 34.3 mW/m^2 (28 to 40 mW/m^2) from CO_2 emissions due to in-flight fuel burn. Similarly a study of the marginal climate and air quality costs of aviation found that contrails produce $92 (USD 2015; 90% uncertainty range $11 to $260) of climate damage per metric ton of fuel burned, compared to $140 ($21 to $360) from CO_2 (Grobler et al., 2019). Although recent studies have suggested that contrails may produce smaller long-term changes in global surface temperature per unit of radiative forcing than previously assumed (Bickel et al., 2025), this does not change the conclusion that contrail impacts are likely to be large enough to warrant low-cost mitigation strategies — as long as the net benefits can be accurately predicted (Borella et al., 2024).

Accordingly, there have been several studies using models to investigate the potential efficacy of different contrail mitigation strategies. Some simply evaluate the potential benefit of using sustainable aviation fuel (SAF) due to the expected

https://doi.org/10.5194/egusphere-2026-4489
Preprint. Discussion started: 13 August 2026

reduction in emitted sulfur and particulates, finding for example that if the number of contrail crystals produced could be reduced by 90% this could yield a 40% reduction in overall contrail radiative forcing (Bier and Burkhardt, 2022; Lottermoser and Unterstrasser, 2026; Rubin-Zuzic et al., 2025). The simulated benefit of all such strategies is subject to our ability to accurately reproduce the overall magnitude of contrail radiative forcing. However, targeted strategies have also been considered. Teoh et al. (2022b) found that, if only 1% of jet fuel worldwide could be replaced with SAF, targeting its use on flights which are expected to form the most climate-warming contrails could reduce net global contrail impacts by 10% and net aviation climate impacts by 6%. Similarly, studies evaluating the potential for contrail formation to be avoided by route deviations – usually vertical, to minimize additional fuel burn and avoid disruption to flight schedules – have suggested that global contrail radiative forcing could be reduced by over 70% at the cost of less than a 1% increase in fuel burn (Gierens, 2025; Martin Frias et al., 2024; Teoh et al., 2020). Despite concerns over the additional CO_2 release, assessments of the net impact of such a strategy using simplified representations of contrail climate impact have found that at least some level of navigational avoidance may be justified regardless of which climate metric was used to evaluate the trade-off (Borella et al., 2024; Smith et al., 2026).

A fundamental challenge in all such assessments is the potential for systematic bias due to model error. Any targeted contrail mitigation strategy fundamentally relies on the assumption that the contrails which cause the most climate warming can be predicted and accurately distinguished in advance from other, less-warming contrails. This requires that the meteorological data be accurate, and that the models used to calculate their climate impacts accurately represent the relationship between local conditions and eventual climate impacts. Given that all current contrail models are either too computationally expensive to be used at scale or make core assumptions which appear to cause disagreement in comparisons against higher-fidelity models, there is an urgent need for new approaches which can compromise between these two extremes.

1.3 Objectives

We confront these challenges using a new, intermediate-fidelity, Lagrangian approach to modeling individual contrails. Section 2 describes the architecture of the model. Section 3 then presents the results of a reference contrail simulation with the model (Section 3.1), followed by a parametric evaluation of meteorological and emission parameters (Section 3.2). Finally, we present a comparison of results from this model against existing literature (Section 3.3) and evaluate the impact of our solution to the aforementioned problem of open energy budgets (Section 3.4) before discussing limitations, implications, and future work (Section 4).

2 Method

To address the issues described above we introduce the Contrail Layer Approximation using Multi-crystal Particles (CLAMP) version 1.0. CLAMP is Lagrangian in nature, tracking a contrail segment from formation to evaporation by

https://doi.org/10.5194/egusphere-2026-4489
Preprint. Discussion started: 13 August 2026

simulating the evolution of a 2-D slice perpendicular to the direction of flight. The contrail is represented using *N* multi-crystal particles ("clusters"), each of which represents a collection of *n* ice crystals. Figure 2 shows the architecture of CLAMP v1.0. Section 2.1 describes the theory of CLAMP's operation, and Section 2.2 describes the specific implementation used in this work.

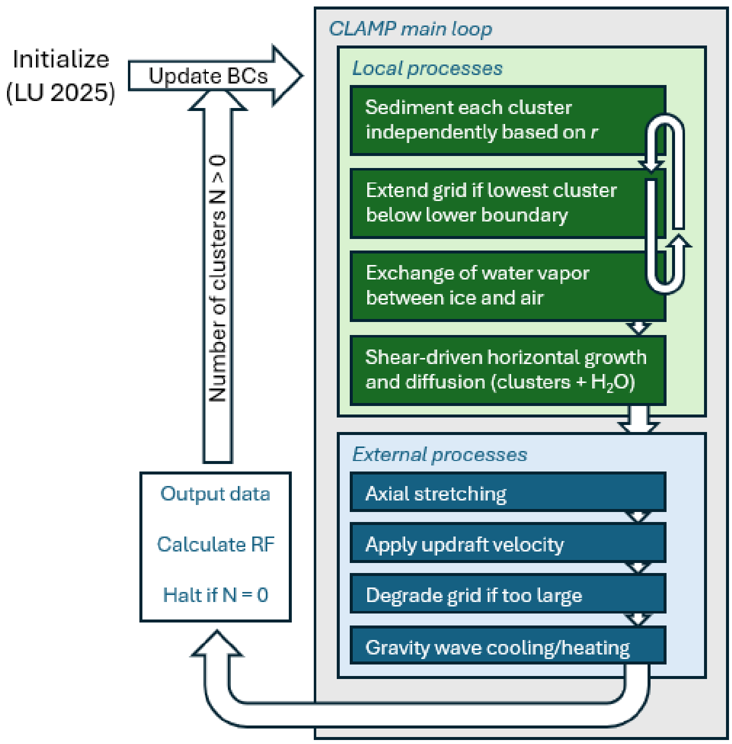

Figure 2. Architecture of CLAMP v1.0. LU 2025 refers to Lottermoser and Unterstrasser (2025), which developed the parameterization from which initial conditions are derived.

2.1 Theory

CLAMP focuses on simulating the post-vortex behavior of the contrail plume, with the assumption that this behavior can be adequately represented without needing detailed simulation of the fluid dynamics. Accordingly the contrail is represented as a two-dimensional cross section of the exhaust plume, initialized as a rectangular, unit-depth volume of air with an approximately uniform concentration of ice crystals – represented as a small number (~1000) of "clusters". A buffer zone of ambient air outside of the contrail is also tracked. Evolution of the plume from this point onwards is controlled by ice crystal growth, wind shear, changes in ambient temperature due to adiabatic compression or expansion, mixing of ambient air into the buffer zones, eddy-driven diffusion, and settling of ice crystals to lower altitudes. Integrating forwards in time, each cluster of ice crystals undergoes growth or sublimation (Section 2.1.1), sedimentation, and horizontal transport due to wind

https://doi.org/10.5194/egusphere-2026-4489
Preprint. Discussion started: 13 August 2026

shear and diffusion. The background water vapor field is equally affected by exchange of water with the clusters, and by horizontal transport due to wind shear and diffusion. The initial and boundary conditions are dictated by an imposed background meteorology (Section 2.1.2), addressing the challenge of how to represent the motion of a contrail segment while retaining internal thermodynamic consistency.

There are three key features of CLAMP which allow it to efficiently capture spatial variability in properties within a contrail. First, the amount and spatial distribution of water vapor in the air is tracked explicitly on a rectilinear grid. This allows differences in relative humidity across the contrail to be represented and preserved over time. Second, the use of a population of clusters to represent the contrail ice means that – for example – phenomena such as spectral ripening (gradual transfer of ice mass from smaller to larger crystals) and gravitational size sorting can be captured. This is similar to the "simulation ice particle" approach used in large eddy simulation (LES) models such as EULAG-LCM, which might use on the order of 10^6 simulation ice particles (i.e. clusters) to represent 10^{12} ice crystals (Unterstrasser and Sölch, 2014). Since the flow fields in CLAMP are much simpler than those of an LES model, a smaller number of clusters (typically 1,500) can be used to represent the same number of crystals. Finally, the contrail is defined by a "hull" (in this case, the convex hull) around all the remaining clusters, with the air inside the hull discretized and allocated to the nearest contrail cluster.

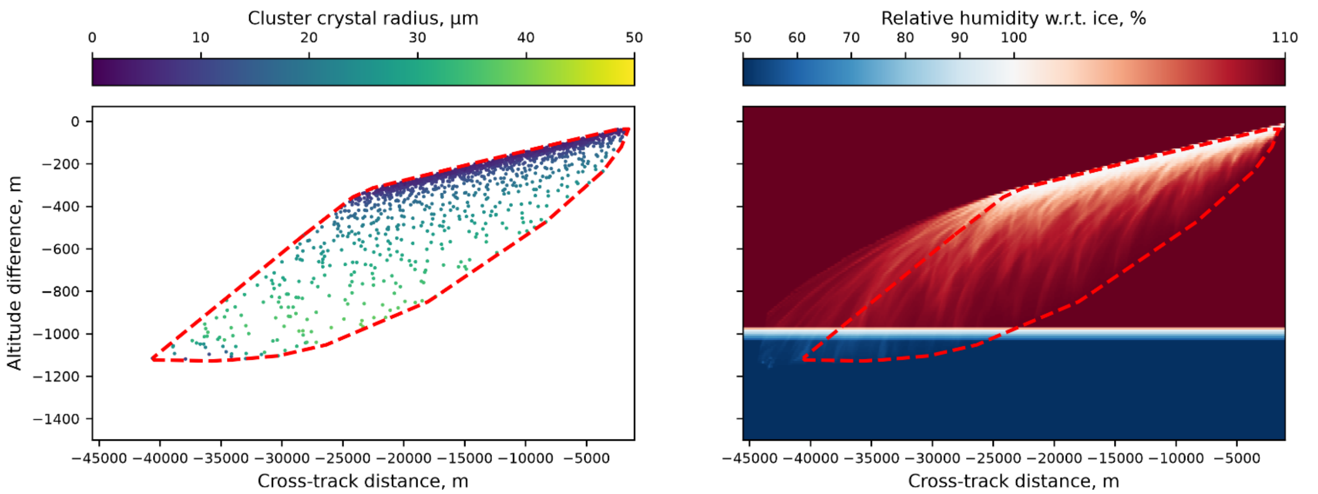

Figure 3. Cross section of a typical contrail in CLAMP after one hour and forty minutes of simulated time. Both panels show data from the same contrail, initially formed at location (0,0). The horizontal axis represents horizontal distance perpendicular to the direction of flight, while the vertical axis represents vertical distance relative to the original altitude of the flight. The red dashed line indicates the boundary of the contrail hull. Left: locations of the cluster centers, with color indicating the radius of all crystals in a given cluster. Right: relative humidity with respect to ice throughout the domain.

These features are demonstrated in Figure 3 for a contrail which has formed in a supersaturated layer (110% above -1000 m, 50% below) and evolved for a further one hour and forty minutes. The use of crystal clusters (left) allows gravitational sorting to occur, with clusters containing larger crystals settling to lower altitude more rapidly. Meanwhile the choice to

https://doi.org/10.5194/egusphere-2026-4489
Preprint. Discussion started: 13 August 2026

represent water vapor on a discretized grid (right) means that the different crystals have access to different amounts of water. Rate-limited crystal growth and sublimation means that, even though all locations within the hull are participating in water exchange with at least one cluster, there is spatial variability in relative humidity across the contrail. The ability of ice clusters to move relative to the air also explains why humidity is reduced outside of the hull, as clusters settle relative to the air and then sublimate upon reaching the subsaturated layer.

2.1.1 Representing contrail dimensions and the exchange of water between air and crystals

Whereas ice crystals are represented by discrete clusters with each centroid stored as a continuous variable, we simulate the motion and composition of background air using a conventional, discretized Eulerian grid. This mirrors the approach used by EULAG-LCM, a large eddy simulation model (Unterstrasser and Sölch, 2014), but with greatly reduced complexity.

At each time step, we define a bounding shape ("hull") which encapsulates all remaining crystal clusters. This is assumed to be the "contrail volume", within which all water exchange between the grid and the contrail crystals takes place. Grid cells are identified as being within the contrail if they contain at least one cluster centroid, or if the grid cell center lies within the hull. Cells which contain no clusters are assigned to the closest cluster using a nearest-neighbor search. If so desired, a scaling factor can be applied during this search so that vertical separation is scaled up (e.g. a scaling factor of five would mean that a vertical distance of 1 m is treated as equivalent to a horizontal distance of 5 m, regardless of the grid resolution). This implies an expectation that horizontal variation in cluster properties is smaller than vertical variation. Cells which contain more than one cluster are allocated to all *n* clusters which will be treated as being in competition for the water within that cell, but it is assumed that each cluster occupies only a fraction (1/*n*) of that grid cell's volume.

Once cell allocation is complete, a system of ordinary differential equations (ODEs) is set up to simulate water exchange following the formulations for ice crystal growth as described by Lohmann et al. (2016) with the addition of a term to describe the Kelvin effect. In a system where n_i ice crystals are interacting with n_j grid cells, the general equation for the rate of change of mass of cluster i interacting with the air in grid cell j is

$$\frac{dm_i}{dt} = n_{i,j} \times C_i \times \frac{4\pi\alpha_{i,j}}{F_{k,\text{ice}} + F_{d,\text{ice}}}\left(s_j + 1 - \exp\left(\frac{a_{k,j}}{r_i}\right)\right) \quad (1)$$

where $n_{i,j}$ is the number of crystals from cluster i present in cell j, C_i is the capacitance of the crystals (a function of habit and radius), $\alpha_{i,j}$ is the accommodation coefficient for cluster i given the conditions in cell j, s_j is the supersaturation in cell j with respect to ice such that $s_j + 1$ is the relative humidity with respect to ice, $a_{k,j}$ is the critical radius in cell j (the k in this instance referring to "Kelvin effect", rather than being an index) and r_i is the volume-weighted mean radius of the crystals in cluster i. The exponential term represents the Kelvin effect, which introduces a dependence of the saturation vapor pressure

https://doi.org/10.5194/egusphere-2026-4489
Preprint. Discussion started: 13 August 2026

on crystal radius and has previously been found to reduce the lifetime of contrails by accelerating crystal losses, especially early in the contrail lifetime (Lewellen, 2012). The critical radius is calculated as

$$a_{k,j} = \frac{2\sigma}{\rho_{\mathrm{ice}} R_v T_j} \tag{2}$$

where σ is the surface tension at the ice/air interface in J m^{-2} (see Appendix A), ρ_{ice} is the density of ice (assumed to be 917 kg m^{-3}), R_v is the specific gas constant for water vapor in J kg^{-1} K^{-1}, and T_j is the temperature in Kelvin within grid cell j. This formulation of the rate of change of ice mass implicitly assumes that all crystals in the cluster have the same radius, although it could be adapted to consider a polydisperse size distribution. This would however increase computational cost and require additional consideration of issues such as different settling velocities for the crystals making up a single cluster.

The factors $F_{k,\mathrm{ice}}$ and $F_{d,\mathrm{ice}}$ represent the effects of latent heat release and vapor diffusion respectively as

$$F_{k,\mathrm{ice}} = \left(\frac{L_s(T)}{R_v T} - 1\right)\frac{L_s(T)}{K(T) \cdot T} \tag{3}$$

$$F_{d,\mathrm{ice}} = \frac{R_v T}{D_v(p,T) e_{s,i}(T)} \tag{4}$$

where L_s is the latent heat of sublimation, K represents the thermal conductivity of air, D_v is the water vapor diffusion coefficient, and $e_{s,i}$ is the saturation vapor pressure of water with respect to ice. The temperature T and ambient pressure p are ideally defined at the location of the relevant cluster's centroid. The approximations used for each of these factors in our implementation are given in Appendix A.

Given that the nature of the Kelvin effect for ice crystals is uncertain and its inclusion increases the complexity of the ice growth calculations, it may be preferable to neglect it. This choice, along with the determination of $\alpha_{k,j}$ and capacitance C_i, is considered implementation-dependent and is therefore discussed in Section 2.2.5.

With the governing equations known, Equation (1) can be extended to consider a single crystal cluster interacting with multiple different grid cells. If we assume that the crystals of a given cluster are evenly spatially distributed over some limited volume (area) and denote the number of grid cells in the domain as N_j, then the total rate of change of mass can be expressed as

https://doi.org/10.5194/egusphere-2026-4489
Preprint. Discussion started: 13 August 2026

$$\frac{dm_i}{dt} = \frac{C_i n_i}{\sum_j A_j \phi_{i,j}} \sum_{j=1}^{N_j} A_j\, \phi_{i,j} f_j \left(s_j + 1.0 - \exp\left(\frac{a_{k,j}}{r_i}\right)\right) \tag{5}$$

where A_j is the volume (area) of grid cell j, $\phi_{i,j}$ is the fraction of grid cell j containing crystals from cluster i, f_j is a grid cell-specific factor (see below), and n_i is the total number of crystals represented in cluster i. The summation in the denominator of the opening term is therefore simply the total volume (area) occupied by the cluster, and the term $A_j\phi_{i,j}$ is the volume (area) of grid cell j containing crystals from cluster i. In practice the summation only needs to include grid cells which have a non-zero contribution from cluster i.

Assuming that the accommodation coefficient $\alpha_{i,j}$ can be calculated as a function of grid cell properties only (i.e. it becomes α_j), the factor f_j becomes

$$f_j = \frac{4\pi\alpha_j}{F_{k,\mathrm{ice}} + F_{d,\mathrm{ice}}} \tag{6}$$

thus gathering the terms from equation (1) which do not depend on the cluster properties. This also requires that F_k and F_d can be approximated using the grid cell mean temperature and pressure, rather than the specific value at each cluster centroid.

At this point it is convenient to express the supersaturation s_j in terms of the mass of water vapor in the grid cell m_j, as this will facilitate development of an expression for mass conservation between the cluster and participating grid cells. The rate of change of relative humidity with respect to ice ($\mathrm{RH_i}$) per unit mass of water in the grid cell can be expressed as

$$\frac{d\mathrm{RH}_{\mathrm{i},j}}{dm_j} = \zeta_j = \frac{R_v T_j}{A_j e_{s,j}} \cdot \frac{1}{L} \tag{7}$$

with L being the depth of the grid cell (i.e. one meter). This means that we can express the supersaturation as

$$s_j = m_j \zeta_j - 1 \tag{8}$$

and therefore rewrite equation (5), assuming unit depth of the grid cell, as

https://doi.org/10.5194/egusphere-2026-4489
Preprint. Discussion started: 13 August 2026

$$\frac{dm_i}{dt} = \frac{C_i n_i}{\sum_j A_j \phi_{i,j}} \left(\sum_{j=1}^{N_j} A_j f_j m_j \zeta_j - \sum_{j=1}^{N_j} A_j f_j \exp\left(\frac{a_{k,j}}{r_i}\right) \right) \tag{9}$$

with the role of the Kelvin effect now separated out in the final (exponential) term. In the limit that the critical radius is much smaller than the cluster ice crystal radius, the exponential term becomes one and the Kelvin effect can be neglected.

By conservation of mass, the rate of change of water in any grid cell j can be expressed by summing the contributions from all clusters which are entirely or partially overlapping with that grid cell. Specifically,

$$\frac{dm_j}{dt} = -A_j f_j \sum_{i=1}^{N_i} \frac{n_i C_i \phi_{i,j} \left(m_j \zeta_j - \exp\left(\frac{a_{k,j}}{r_i}\right)\right)}{\sum_k^{N_i} A_k \phi_{i,k}} \tag{10}$$

where the summation in the denominator now represents the total volume (area) over which cluster i is spread, such that n_i divided by this factor yields the average number concentration of crystals. Multiplying this by A_j and $\phi_{i,j}$ then yields the total number of crystals from cluster i interacting with grid cell j.

At this point, it is necessary to convert elements which are functions of the crystal radius r into functions of the cluster mass m_i. We first assume that the capacitance can be expressed as

$$C_i = k \cdot r_i \tag{11}$$

where k is a habit-dependent factor. Unless otherwise specified we assume that the crystals are functionally spherical, such that $k = 1$; this could, for example, be replaced with $k = 2/\pi$ to represent plate-type crystals (Lohmann et al., 2016). The relationship between mass and radius is then expressed as

$$m_i = n_i \left(\frac{4}{3} \pi r_i^3 \rho \right) \tag{12}$$

where ρ is the mass density of ice (917.0 kg m^{-3}). We can isolate quantities that are dependent only on crystal and cell properties into leading factors that we denote γ and β respectively. This allows the rate of change of mass of each cluster to be represented as

https://doi.org/10.5194/egusphere-2026-4489
Preprint. Discussion started: 13 August 2026

$$\frac{dm_i}{dt} = \gamma_i m_i^{\frac{1}{3}} \left(\sum_{j=1}^{N_j} \beta_j m_j \zeta_j - \sum_{j=1}^{N_j} \beta_j \, exp\left(a_{k,j} \left(\frac{3m_i}{4\pi n_i \rho} \right)^{\frac{1}{3}} \right) \right) \tag{13}$$

and the rate of change of mass of each grid cell to be represented as

$$\frac{dm_j}{dt} = \beta_j \sum_{i=1}^{N_i} \left(\exp\left(a_{k,j} \left(\frac{3m_i}{4\pi n_i \rho} \right)^{\frac{1}{3}} \right) - m_j \zeta_j \right) \gamma_i m_i^{\frac{1}{3}}, \tag{14}$$

with γ_i determined by expressing C_i as a function of m_i such that

$$\gamma_i = \frac{C_i n_i}{\sum A_j \phi_{i,j}} = \frac{1}{\sum A_j \phi_{i,j}} \left(\frac{3n_i^2}{4\pi\rho} \right)^{\frac{1}{3}}. \tag{15}$$

Here the denominator is again simply the total volume (area) occupied by cluster i. Similarly we gather the terms which are functions of the cell only into the new factor $\beta_j = A_j f_j$.

This provides a system of $N_i + N_j$ coupled ordinary differential equations which can be integrated forwards in time to simulate the exchange of water between clusters and grid cells. If the Kelvin effect can be neglected, these simplify to

$$\frac{dm_i}{dt} = \gamma_i m_i^{\frac{1}{3}} \sum_{j=1}^{N_j} \beta_j (m_j \zeta_j - 1) \tag{16}$$

and

$$\frac{dm_j}{dt} = \beta_j (1 - m_j \zeta_j) \sum_{i=1}^{N_i} \gamma_i m_i^{\frac{1}{3}} \tag{17}$$

respectively.

https://doi.org/10.5194/egusphere-2026-4489
Preprint. Discussion started: 13 August 2026

2.1.2 Evolution of ambient conditions over time

The above processes are simulated within an isolated two-dimensional domain, typically up to 50 km wide and 1-2 km tall. An arbitrary depth (segment length) is assumed, allowing for stretching and compression of the segment (see e.g. Section 2.2.7). The boundary conditions for this domain can however evolve over time due to the large-scale motion of the domain itself. This can include horizontal advection of the domain, vertical advection due to synoptic-scale motions, vertical motions due to gravity waves, or gradual changes in boundary conditions as the air near to the contrail mixes with air from other sources. This latter factor can affect the simulated contrail as the tracked area expands (e.g. if any ice clusters descend below the initial vertical limit) and as air is brought into the tracked area through horizontal shear (see Figure 4). Time-varying boundary conditions are therefore needed, even though the conditions within the tracked volume maintain internal consistency and will evolve only due to explicitly resolved mass and heat transfer processes. The approach described here is intended to resolve, to the greatest extent possible, the inconsistency described in Section 1.1 between the Eulerian grid of ambient conditions and the Lagrangian approach to modelling contrail evolution.

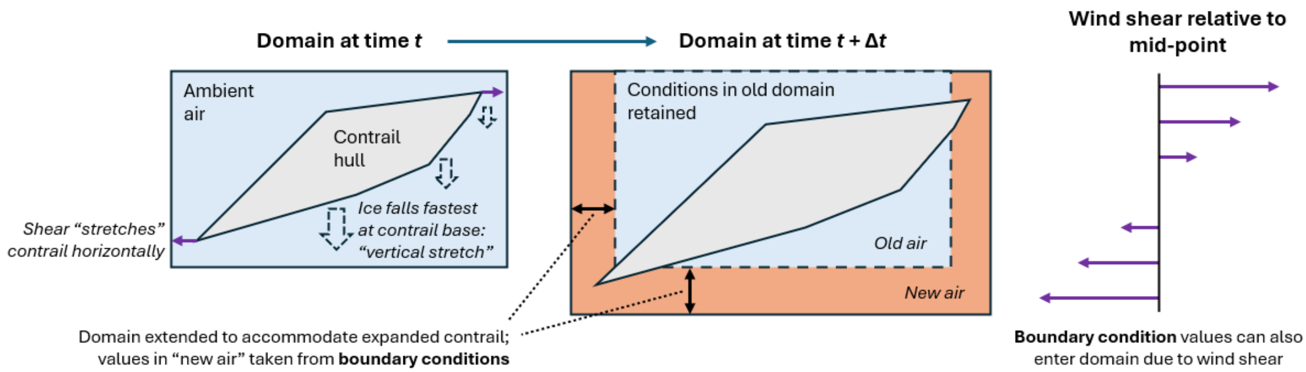

Figure 4. Schematic illustrating mechanisms by which changing boundary conditions can enter the tracked domain. Shear and differential settling speeds act to increase the horizontal and vertical width of the contrail respectively, such that the domain at time *t* (left panel) has to expand to accommodate the contrail at time *t* + Δ*t* (middle panel). The conditions in this expanded region are taken from the ambient boundary conditions. Air with boundary condition properties can also enter the domain due to wind shear (right panel). The effect of vertical winds is not shown, as this changes the internal and boundary conditions directly.

We first consider synoptic-scale motions and changes. As with the CoCiP model, these can be represented by performing a trajectory calculation using data from a meteorological reanalysis such as the European Centre for Medium Range Weather Forecasts (ECMWF)'s ERA5, yielding a timeseries of ambient temperature, pressure-velocity, and specific humidity (Schumann, 2012). Such trajectory calculations can be achieved using (for example) the dry advection facility within the pycontrails Python module (DOI: 10.5281/zenodo.17944440) and are not described here. Since CLAMP internally models variability of internal, boundary, and initial conditions with altitude, it is useful to extract a curtain of ambient conditions with dimensions of altitude and time rather than just the 1-D timeseries of conditions along the trajectory. For the purposes

https://doi.org/10.5194/egusphere-2026-4489
Preprint. Discussion started: 13 August 2026

of determining the relationship between the curtain coordinates and the CLAMP internal coordinates it is assumed that the location (0,0) within the internal CLAMP domain (see Figure 3) corresponds to the location and altitude of the advected air parcel.

The fact that the CLAMP domain is internally discretized means that changes in the ambient specific humidity do not immediately propagate to the contrail core. Instead, these changes are imposed only at the boundaries of the contrail domain. Where this boundary is imposed is an implementation choice, reflecting a fundamental inconsistency between Lagrangian and Eulerian modeling approaches. The approach used in our implementation is described in Section 2.2.4.

Models such as CERM and CoCiP assume that the temperature at the new location should be imposed on the contrail, modifying the relative humidity within the contrail core (Caiazzo et al., 2017; Schumann, 2012). However, this approach implicitly allows temperature changes due to mixing far from the contrail to propagate instantaneously to the contrail core. As discussed in Section 1.1, it also results in an open energy budget; changes in the contrail are the result of whatever processes drove changes in the grid-scale temperature, which may or may not be relevant at the scale of an individual air mass.

In CLAMP, we instead enforce a closed energy budget where changes in temperature occur only because of explicitly resolved sources of heating. These can be separated into adiabatic (compression and expansion due to synoptic-scale vertical motions) and diabatic (due to either radiative cooling or latent heat release during phase changes) heating. Adiabatic heating has previously been identified as a controlling influence on contrail lifetime (Hofer and Gierens, 2025) and is thus prioritized, although under some circumstances diabatic heating may be dominant and/or may be strongly coupled to the rate of adiabatic heating (Nie and Sobel, 2016; Sobel et al., 2001).

At initialization, CLAMP adopts an initial temperature profile which is defined on a set of levels. These levels all undergo simultaneous vertical motion based on the synoptic-scale updraft velocity, such that the pressure at time t on level i is $p_i(t)$ and temperature is $T_i(t)$. As the simulation progresses the pressure at each level evolves as

$$p_i(t) = p_i(0) + \int_0^t \omega \, dt \quad (18)$$

where ω is the overall pressure velocity of the air mass. The same pressure evolution is applied to the grid cell boundaries defining the CLAMP internal domain. Changes in temperature due to adiabatic heating are calculated at each level by assuming that the air is an ideal gas undergoing isentropic compression or expansion. Accordingly, the temperature change at level i can be calculated as

https://doi.org/10.5194/egusphere-2026-4489
Preprint. Discussion started: 13 August 2026

$$\Delta T_i = \int_t^{t+\Delta t} \left(\frac{dT_i}{dt}\bigg|_{\mathrm{a}} + \frac{dT_i}{dt}\bigg|_{\mathrm{d}} \right) dt = T(p_i, t) \times \left(\left(1 + \frac{\Delta p}{p_i(t)} \right)^{\frac{\gamma - 1}{\gamma}} - 1 \right) + \int_t^{t+\Delta t} \frac{dT_i}{dt}\bigg|_{\mathrm{d}} dt \quad (19)$$

where γ is the ratio of specific heats for dry air, and $\frac{dT_i}{dt}\Big|_{\mathrm{a/d.}}$ is adiabatic (a) or diabatic (d) heating. The result is that the mapping between pressure and temperature evolves over time within the air mass, but is defined entirely by the initial vertical profile and subsequent contributions from explicitly-resolved sources of heating. In the absence of diabatic heating this means that each level follows an isentrope, rather than remaining at a fixed pressure. Any changes in the temperature sampled from the meteorological boundary condition data (the "boundary temperature") after initialization have no effect on the temperature profile within the domain.

Wind shear and horizontal diffusion mean that we must also account for changes in humidity at the horizontal boundaries of the domain. These boundary conditions are initially set based on the meteorological vertical profile supplied to the model. Changes in the boundary wind shear, relative humidity, and synoptic-scale updraft velocity can be imposed easily, although divergence due to non-uniformity in vertical velocity across the CLAMP domain is neglected. However, humidity must be handled carefully. A set of choices must be made regarding how to handle independent changes in the boundary temperature, boundary relative humidity, and in-domain temperature profile. The choices made in our implementation are discussed in Section 2.2.4, and the consequences of this are explored in Section 3.4.

Finally, vertical motions due to gravity waves require specialized treatment. These waves are likely not to be explicitly resolved by the meteorological models from which boundary conditions are calculated, but the temperature fluctuations induced through adiabatic compression and expansion (equation 19) have been shown to modulate contrail lifetimes (Kärcher and Corcos, 2025). A stochastic representation of the effect of unresolved gravity waves is therefore needed. Our implementation of such a treatment is discussed in Section 2.2.10.

2.2 Implementation

We implement CLAMP v1.0 in Python 3.12.13 (https://www.python.org/downloads/release/python-31213/), leveraging NumPy 2.4.3 (https://pypi.org/project/numpy/2.4.3/) (Harris et al., 2020) and SciPy 1.17.1 (https://pypi.org/project/scipy/1.17.1/) (Virtanen et al., 2020). The code is publicly available at https://github.com/ICL-AEIS/fallstreak. A contrail simulation with CLAMP takes place through four steps. First, the mature contrail is initialized using parameterizations to estimate the post-vortex ice crystal concentration and spatial distribution (Section 2.2.1). Subsequently the contrail extent and properties are estimated by iterating forward in time until no crystals remain (Section 2.2.2), storing relevant output data as necessary (Section 2.2.11). Finally, the stored output from the contrail is provided to a

https://doi.org/10.5194/egusphere-2026-4489
Preprint. Discussion started: 13 August 2026

linearized radiative transfer model to estimate the radiative forcing, and therefore climate impact, resulting from the contrail's formation (Section 2.2.12).

2.2.1 Contrail initialization and grid specification

Since CLAMP is designed to simulate only the mature plume (dispersion) phase of a contrail, we apply parameterizations of the jet and vortex phases to determine the dimensions of the contrail and the total number of surviving crystals once the wing-tip vortices have dispersed (Kärcher, 2018). We calculate the number of particles emitted per meter N_P as

$$N_P = \frac{\dot{m}_f}{V} \cdot \max(\mathrm{EI_n}, 10^{13}) \tag{20}$$

where V is the flight speed in m s^{-1}, $\dot{m}_f$ the fuel flow rate from all engines in kg s^{-1}, and $\mathrm{EI_n}$ the soot number emissions index in particles per kg of fuel. A lower bound of 10^{13} particles per kg is applied, as simulations of aerosol microphysics have suggested that ambient aerosol and formation of volatile particulate matter will result in this many particles being available even when soot emissions are further reduced (Kärcher, 2018; Ponsonby et al., 2025; Teoh et al., 2022b).

We first check that the Schmidt-Appleman criterion is satisfied by estimating the threshold temperature T_{SAC} using the procedure from Bräuer et al. (2021) and verifying that it is greater than the ambient temperature T_{amb}. The pre-vortex ice crystal number count per unit flight distance N_{C0} is then estimated as

$$N_{C0} = N_P \cdot p_{\mathrm{activation}} \tag{21}$$

where the activation fraction $p_{\mathrm{activation}}$ is calculated following Teoh et al. (2022a) as

$$p_{\mathrm{activation}} = 1 - 0.661 \exp(T_{\mathrm{amb}} - T_{\mathrm{SAC}}) \tag{22}$$

to account for potentially incomplete particle activation as a function of ambient temperature and humidity (Bräuer et al., 2021).

The post-vortex horizontal extent W, vertical extent D, and survival fraction f_{NS} are estimated using the young contrail parameterization described in Lottermoser and Unterstrasser (2025), which provides these quantities at a point six minutes after passage of the aircraft. W is calculated using the area-equivalent width $W_{\mathrm{rect}} = 0.63b$, where b is the aircraft wingspan, as this produces a contrail where the mean number concentration of crystals is more realistic than if the "true" width is used (Unterstrasser, 2016). The post-vortex ice crystal count N_C is then calculated as the survival fraction multiplied by the pre-

https://doi.org/10.5194/egusphere-2026-4489
Preprint. Discussion started: 13 August 2026

vortex crystal count N_{C0}. The original parameterization was fit to data where the maximum value of N_{C0} was 3.38×10^{14} m^{-1}, and inputs which generate a higher value within the parameterization can cause f_{NS} to fall so low that increasing EI_n results in a decrease in N_C. To avoid this behavior, we do not allow the parameterization to extrapolate into this regime and instead use the closest valid value of f_{NS} for very high ice crystal counts. This is not an issue for low values of N_{C0} as, in these cases, f_{NS} tends to 1.

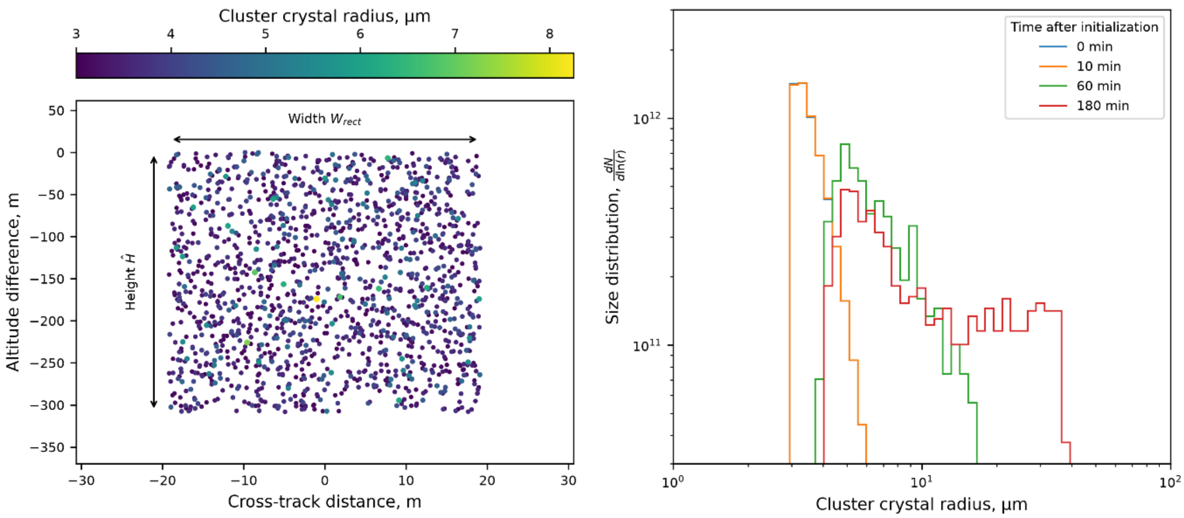

Figure 5. Properties of the contrail shown in Figure 3. For the example shown, the number of multi-crystal particles N_P = 1500. Left: spatial distribution of ice crystals at initialization, with dimensions corresponding to distance from the initial emission point. Right: size distribution within the contrail at initialization (following the vortex phase, during which water uptake and elimination of small crystals is parameterized), and after 10, 60, and 180 minutes of contrail evolution.

The crystals are evenly distributed among N_i multi-crystal particles, each of which is assigned a random coordinate within the contrail area. The contrail is initialized such that its uppermost limit is at the original flight pressure-altitude (y = 0) with the lowermost extent at y = $-D$ meters, with particle vertical locations chosen randomly over this range. In the cross-track coordinate, particles are initialized at random locations between ±0.5 W meters. A seed can be specified for the random number generator if desired to ensure reproducibility. The impact of randomness is in general small unless stochastic gravity wave forcing is included (see Section 2.2.10 for more details, and Section 3.2.3 for evaluation of the impact of randomness with and without gravity waves).

The total mass of the initial ice crystal distribution is estimated by assuming first that all water emitted from the aircraft exhaust will freeze onto the ice crystals which survived the vortex phase, and that subsequently the relative humidity within the contrail volume will reach 100% by the time that the vortices have dissipated. This is on the assumption that air is well

https://doi.org/10.5194/egusphere-2026-4489
Preprint. Discussion started: 13 August 2026

mixed within the vortex system and that five minutes is long enough to reach equilibrium, subject to verifying that the combined (emitted and ambient) water mass is sufficient to saturate the air within the vortex system. Accordingly all cells within the hull are initially brought to 100% relative humidity, and the excess water is assumed to be taken up as ice on the available ice crystals. The mass of soot within the contrail ice is neglected, considering that typical soot and water emissions indices are 8.80×10^{-5} and 1.24 kg/kg respectively (Teoh et al., 2024b). As such, the mass of soot emitted per kilogram of fuel burned is expected to be at least four orders of magnitude less than the mass of water emitted.

The resultant population of ice crystals is assigned a log-normal size distribution to represent inhomogeneity in particle activation and behavior during the turbulent jet and vortex phases. By default we use a geometric standard deviation of 2.85, consistent with a width parameter r_{SD} = 3 (Unterstrasser, 2014; Unterstrasser and Sölch, 2010). The distribution is first applied using the total number of ice crystals N_{C0}, after which it is assumed that the smallest crystals are lost to vortex sinking such that only the fraction f_{NS} remain. This crudely represents the process observed in LES studies during the vortex sinking phase (Lewellen et al., 2014; Unterstrasser and Sölch, 2010). The ice mass from these smallest particles is then redistributed proportionally to the remaining particles, resulting in a truncated log-normal distribution. The result for a typical contrail is shown in Figure 5, which demonstrates how the distribution has been truncated to eliminate crystals with a radius below 3.0 µm.

2.2.2 Operations performed each time step

Once the domain is initialized, the simulation is integrated forwards in time using a user-imposed time step Δt, updating the boundary conditions as necessary when local meteorological conditions change. All times are reported in terms of seconds, minutes, or hours since the beginning of the simulation, which represents the contrail approximately six minutes after passage of the aircraft (Lottermoser and Unterstrasser, 2025).

Within a single time step, the following procedure is performed. First, an inner loop is simulated in which only settling, grid extension, and water exchange take place. For this inner loop the remaining time Δt_{rem} is compared to the maximum settling speed of any individual cluster divided by the vertical grid spacing, yielding Δt_{max}. If Δt_{rem} exceeds Δt_{max} then a shorter time step of length Δt_{max} is taken, to avoid any clusters settling through a grid cell without interacting with it. As long as the total number of remaining clusters N_i is still greater than zero, CLAMP then performs the following steps in each inner loop: gravitational settling of crystals (Section 2.2.3); extension of the grid to ensure the domain contains all crystals and any air which those crystals will interact with (Section 2.2.4); and exchange of water between the crystals and ambient air (Section 2.2.5). Once these operations are completed, another inner time step is taken until the full time step Δt is completed. Following the example of Lewellen et al. (2014) and Unterstrasser (2014) we neglect aggregation of ice crystals, as this process is expected to be negligible at contrail temperatures (Connolly et al., 2012).

https://doi.org/10.5194/egusphere-2026-4489
Preprint. Discussion started: 13 August 2026

Once this inner loop is complete, advection and diffusion of both water vapor and crystals are calculated (Section 2.2.6). This is followed by modification of the grid to account for stretching of the contrail segment (Section 2.2.7), and adjustment of the domain temperature profile to account for the effect of synoptic-scale updrafts (Section 2.2.8). Finally, the effect of domain growth on the number of grid cells being simulated is evaluated and, if necessary, the grid resolution is degraded to constrain the computational cost of the simulation (Section 2.2.9). The effect of mesoscale gravity waves is imposed as a domain-wide adjustment to the temperature, calculated once per outer time step (Section 2.2.10).

Simulation output is stored at a lower frequency per a user-defined diagnostic time step (Section 2.2.11). Radiative transfer calculations can be performed either as part of this data storage process or using archived output (Section 2.2.12), allowing the instantaneous radiative forcing of a given contrail to be estimated.

2.2.3 Gravitational settling of crystals

Gravitational settling of crystals is calculated using a simple Stokes law approach. All crystals in a given cluster are assumed to fall at the same speed, calculated as the terminal velocity V_{fall} for a sphere of ice with a mass density of 917 kg m^{-3}. Using the radius r_i for cluster i in meters, the velocity is therefore calculated as

$$V_{\text{fall}} = \frac{2r_i^2(\rho_{\text{ice}} - \rho_{\text{air}})g}{9\mu} \tag{23}$$

where g is the gravitational acceleration (9.81 m s^{-2}), ρ_{air} is the mass density of air (kg m^{-3}) calculated using the ideal gas law, and μ is the dynamic viscosity (Pa s) approximated as shown in Eq. A6. We neglect molecular slip on the basis that the Knudsen number is expected to be small for these conditions and crystal sizes. Similarly we do not account for the effect that different crystal habits could have on fall velocities. Although such a change would be straightforward to implement using (for example) the fall speed relationships described by Heymsfield and Westbrook (2010), our growth model also does not currently account for non-spherical crystals. As such we choose to use a spherical model for all ice microphysics in the current version of CLAMP. Within the inner loop (Section 2.2.2) vertical displacement of each cluster by gravitational settling is calculated using first order accurate forward Euler integration, such that $\Delta y = -V_{\text{fall}}\Delta t$ where y is defined as the vertical dimension (i.e. altitude).

2.2.4 Grid extension and boundary conditions

When the model domain is extended or when air crosses the domain boundary, a 1D vertical profile of water molecular concentrations must be provided. We choose to do so by storing the user-provided meteorological profile of relative humidity, and deriving the implied specific humidity. This specific humidity is then used to derive future boundary relative humidities. If the contrail advects vertically due to synoptic-scale motions (i.e. updrafts and downdrafts), the specific

https://doi.org/10.5194/egusphere-2026-4489
Preprint. Discussion started: 13 August 2026

humidity profile moves with it to simulate the effect of the entire air mass moving coherently. Following the terminology established in Section 2.1.2, the specific humidity at the boundary is preserved on each level and the boundary relative humidity recalculated as the temperature evolves.

If however an update is provided for the boundary condition (e.g. the contrail-carrying air mass is carried into a new region), the boundary relative humidity is updated and the boundary specific humidity is calculated based on the in-domain temperature profile. This compensates for the fact that we do not track temperature in 2D. For example, if the domain has risen and therefore cooled adiabatically to a greater degree than its surroundings, we should in theory have warmer air entering at the boundaries carrying more water for a given relative humidity than is the case for the colder air in the domain. Since this is not possible with CLAMP's current architecture, we instead simply ensure that the air is supersaturated to the correct relative factor for the local temperature. This is demonstrated in Section 3.4.

2.2.5 Water uptake

As described in Section 2.1.1, CLAMP requires a method to determine the hull (i.e. bounding limit in 2D) of the clusters and to then determine the relationship between the clusters themselves and the finite volume grid on which air properties (including water vapor concentration) are stored. In this implementation, we use SciPy to build a *k*-dimensional tree for nearest-neighbor lookup (scipy.spatial.KDTree) and we define the hull as the convex hull, calculated using Qhull (Barber et al., 1996) within SciPy (scipy.spatial.ConvexHull). The convex hull is chosen as the bounding shape due to the existence of methods for its rapid calculation, but also means that there is likely to be some spurious water uptake when the outline of the contrail is concave. Future implementations may wish to consider the use of alternatives such as alpha shapes (Edelsbrunner et al., 1983).

Generation of the *k*-dimensional tree is performed with a vertical scaling of 5 by default, meaning that vertical distances are inflated by a factor of 5 for nearest-neighbor calculation and thus biasing water exchange to occur horizontally rather than vertically. By splitting the settling and ice growth operators, we ensure that the cell assignments only need to be determined once per time step and thereby avoid repeated construction of the system of ordinary differential equations (ODEs) described in Section 2.1.1. The hull generation and cell assignment for this implementation of CLAMP is shown schematically in Figure 6.

https://doi.org/10.5194/egusphere-2026-4489
Preprint. Discussion started: 13 August 2026

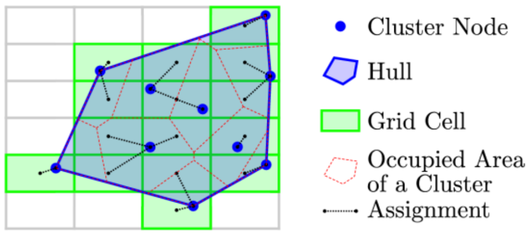

Figure 6. Grid assignment approach in this implementation of CLAMP. The 10 blue "cluster nodes" correspond to the ice crystal clusters making up the contrail, while 6 × 4 set of "grid cells" correspond to the finite volumes of air for which water vapor is tracked. Green grid cells are included in water exchange with one or more clusters, whereas white cells are considered to be "outside" the contrail. This case is illustrative only, as a CLAMP contrail is typically represented using O(1000) clusters and would encompass hundreds to thousands of grid cells.

An additional, optional performance improvement involves the use of block assignment. Simulation speed can be accelerated by grouping air volumes together in sets of 3×3 or 5×5 during water exchange, reducing the number of independent equations which need to be solved. This is functionally similar to degrading the grid resolution but allows certain quantities to be retained at higher resolution.

Once cell assignment is complete, the system of ODEs is constructed and integrated forward in time using the "RK23" method within SciPy's solve_ivp function. RK23 implements an explicit Runge-Kutta 3rd-order method with error-control based on a 2nd-order method (Bogacki and Shampine, 1989). The system can be built with or without the Kelvin effect, although a parameterization of the consequences of the Kelvin effect during the jet and vortex phase is included independently in model initialization (Section 2.2.1). Once integration is complete, any clusters with zero or negative mass are eliminated and the resultant mass deficit is taken from the cells to which that cluster was assigned.

During integration of the system, the sublimation and deposition coefficients can be set independently. This can represent the fact that deposition is expected to occur more slowly than sublimation for equivalent super- and sub-saturations (Kärcher et al., 2023). By default, we assume that both the sublimation and deposition coefficients are 0.5 in light of the high degree of uncertainty in both (Lohmann et al., 2016; Spichtinger and Gierens, 2009). Increasing the sublimation coefficient to 1.0 decreases the lifetime integrated surface area density for our reference case by 4.63%.

Three shortcomings of this implementation are the lack of competition, the simplified approach to ice crystal habit, and the lack of ventilation. First, the cell assignment approach described above results in many cells being exclusively assigned to one cluster. This inhibits competition between crystals of different sizes and therefore implicitly dampens any Ostwald ripening effect, which might otherwise broaden the spectrum and result in continuous ice losses (Lewellen et al., 2014; Lewellen, 2012; Unterstraßer et al., 2017). This could be addressed by enabling the Kelvin effect parameterization and developing an alternative approach to crystal assignment, such as inverse distance weighting. However this would incur a

https://doi.org/10.5194/egusphere-2026-4489
Preprint. Discussion started: 13 August 2026

performance penalty by further coupling the ODEs, and prior literature has suggested that the largest effects from spectral ripening occur during the vortex phase as discussed above.

Second, we assume that all crystals are functionally spherical and therefore have a capacitance equal to their radius. Alternative geometries could be trivially approximated by modifying the sublimation and deposition coefficients to include the dimensionless capacitance factor, e.g. by including a factor of 1/π for plates (Field et al., 2008). Similarly, we do not account for the effect that ventilation might have in accelerating ice crystal growth on the basis that this is most significant for large snow crystals and less important for cirrus (Nelson and Knight, 1998).

2.2.6 Horizontal transport of water and particles

Transport is performed independently for the clusters and for gridded fields (i.e. water vapor). All advection assumes piecewise constant volumetric mixing ratio in the source cells, and the horizontal velocity at each altitude $\bar{u}$ is determined by interpolation of the horizontal wind speed from the meteorological boundary condition. Horizontal and vertical diffusivity, D_H and D_V, are assumed to be constant throughout the domain. By default D_H is set to 10 m^2s^{-1}, although this can be modified and sensitivity to this factor is explored in Appendix B. Vertical diffusion is currently ignored in the model (i.e. $D_V = 0$ m^2s^{-1}).

Horizontal transport of gridded data is performed with Strang operator splitting for diffusion and advection. Diffusion over two half-timesteps is performed using backward Euler integration, leveraging the PETSc library for efficiency (Dalcin et al., 2011; USDOE Office of Science (SC), Advanced Scientific Computing Research (ASCR) et al., 2025). Advection is performed using a semi-Lagrangian approach to allow for the high Courant-Friedrichs-Lewy numbers which can arise when applying a large wind shear relative to the starting altitude.

Horizontal transport of clusters is performed independently using a first order forward Euler integration in time. Vertical transport is performed separately as part of the inner loop due to the relationship between fall speed and terminal velocity (see Section 2.2.3). Horizontal advection is calculated by combining the mean wind velocity $\bar{u}$ with an unsteady component u' drawn from a normal distribution with a mean value of zero and a variance of

$$\sigma_x^2 = \frac{2D_H}{\Delta t} \tag{24}$$

where Δt is the outer time step. This approach, described by Bakels et al. (2024) for the model FLEXPART version 11, reproduces the effect that diffusion has on water vapor. Accordingly, the horizontal wind speed for each cluster is calculated by drawing from the distribution $u \sim N(\bar{u}, \sigma_x^2)$.

https://doi.org/10.5194/egusphere-2026-4489
Preprint. Discussion started: 13 August 2026

2.2.7 Accounting for contrail stretching

Whereas wind shear does not change the cross-sectional area of a contrail segment, stretching of the segment along its length does. Following Konopka (1995), we assume that only the horizontal width of the plume is affected by changes in segment length while the vertical extent remains unchanged. This means that there is no work done due to vertical motions, and segment stretching manifests only as a narrowing of the plume.

To implement this, the length of the contrail segment can be provided to CLAMP at each time step. The ratio of the segment length at the end of the time step to that at the start, r_L, is then calculated based on changes in the supplied length between time steps. The horizontal grid spacing and cluster horizontal centroids are then divided by this factor to represent the contraction of the plume. The gridded water vapor concentration in molecules per cm^3 is unchanged; however, since the crystals are tracked in terms of the number of crystals per unit length, the number of crystals per cluster is also divided by r_L.

2.2.8 Updrafts and subsidence

Synoptic-scale subsidence is one of the three primary mechanisms by which contrails evaporate, as the air warms and saturation decreases (Hofer and Gierens, 2025). CLAMP represents this process by accepting vertical velocity w as an input, expressed in cm s^{-1}. We translate w into a pressure velocity, ω (Pa s^{-1}), by assuming that $\frac{dp}{dz} = -\rho g$ which should be appropriate for synoptic-scale motions (Holton, James R.; Hakim, Gregory J, 2012). Accordingly $\omega \approx -\rho g w$ where the local air density ρ is diagnosed from the meteorological boundary conditions using the ideal gas law and g, the local acceleration due to gravity, is assumed to be 9.81 m s^{-2}. With ω known, the rate of change of temperature is calculated throughout the entire domain by assuming adiabatic (isentropic) heating and compression. Accordingly, the temperature at each vertical location within the domain after a time step Δt during which the mean pressure velocity was ω is calculated as

$$T(t + \Delta t, z) = T(t, z) \times \left(1 + \frac{\omega \Delta t}{p(t, z)}\right)^{\frac{\gamma - 1}{\gamma}} \tag{25}$$

where $T(t,z)$ is the temperature at the start of the time step in Kelvin at altitude z, $p(t,z)$ is the pressure at the start of the time step in Pascals at the same altitude, and γ is the ratio of specific heat capacities (assumed to be 1.4). Variation in vertical velocity within the CLAMP domain is neglected, such that one value of ω is applied to the entire domain at each time step. However new values of ω can be supplied at each time step to reflect variation over time.

2.2.9 Adaptive grid resolution

To provide an appropriate representation of the early fine-scale structures while also capturing the scale of mature contrails, we employ an adaptive gridding approach. At the end of each inner timestep (see Section 2.2.2), the size of the domain is

https://doi.org/10.5194/egusphere-2026-4489
Preprint. Discussion started: 13 August 2026

modified to wrap the contrail as tightly as possible. The minimum distance to the edge of the contrail hull is calculated for each of the four domain boundaries, including (for the left and right boundaries) a buffer based on the maximum signed horizontal velocity of any cluster. If this range extends beyond the current domain, additional rows and columns are appended to the grid using the meteorological boundary conditions, adjusted as necessary to account for any synoptic-scale vertical motions which have already occurred (Section 2.2.8). Any rows or columns outside of this range are removed, reducing unnecessary computational cost.

At the end of each outer timestep, an additional check is performed. If the number of columns n_x exceeds a maximum value $n_{x,max}$, the horizontal grid spacing is halved and pairs of columns are combined, avoiding spurious diffusion which might occur if non-integer numbers of columns needed to be successively averaged. If necessary, this process is then repeated until n_x is once again less than or equal to $n_{x,max}$.

2.2.10 Gravity waves

The effect of unresolved gravity waves on each contrail is represented stochastically, following the approach described by Kärcher and Podglajen (2023) and further discussed by Kärcher and Corcos (2025). At initialization a Laplacian distribution is defined with a mean value of 0, scaled by the user-supplied mean fluctuation w' in m s^{-1}. The autocorrelation time of the gravity waves $\Delta t_{\mathrm{auto}} = 1/N$, where N is the user-supplied Brunt-Väisälä frequency. As the simulation proceeds, the time since the last update is monitored; if this time exceeds Δt_{auto} then a new fluctuation magnitude is drawn from the Laplacian distribution, and the gravity wave-induced temperature tendency is calculated as

$$\frac{d\Delta T_{\mathrm{GW}}}{dt} = -\frac{f\Delta T_{\mathrm{GW}} + \Gamma w'}{1 + f\Delta t_{\mathrm{auto}}} \tag{26}$$

where ΔT_{GW} is the current temperature fluctuation across the entire domain due to gravity wave-induced motion, Γ is the dry adiabatic lapse rate (10 K km^{-1}), w' is the mean fluctuation in m s^{-1}, and f is the Coriolis frequency at the given latitude. Unless otherwise specified we assume $N = 0.0115$ rad s^{-1}, $w' = 0.1$ m s^{-1}, and calculate the Coriolis frequency at 60°N resulting in $f = 1.26 \times 10^{-4}$ rad s^{-1}. N and f are overridden based on local ambient conditions and the emission latitude for the calculations in Section 2.2.10. Data on the correct value of w' is sparse, and it is thus treated as a user-defined constant.

2.2.11 Data storage

Output data from CLAMP are stored through its "history" component. At model initialization, the user selects what to output: this can include 0-D (e.g. time, number of ice crystals per meter, contrail area), 1-D (e.g. temperature profile, grid coordinates in each dimension), and 2-D variables (e.g. gridded ice water content, water vapor concentrations). Timeseries

https://doi.org/10.5194/egusphere-2026-4489
Preprint. Discussion started: 13 August 2026

for each cluster can also be output (e.g. mean radius by cluster). If radiative forcing is to be calculated (Section 2.2.12) then the longwave, shortwave, and net forcing can be stored alongside the contrail's effective width, integrated energy forcing, and solar zenith angle. To allow calculation of radiative forcing to be split from simulation of the contrail, the key radiative forcing state variables can also be output.

As the simulation proceeds, the data for each variable are stored once at initialization and then once per storage time step. Once the simulation is complete all data can be serialized using NumPy. Serialized data can then be used to initialize a standalone history component, facilitating the use of identical workflows for data from ongoing or archived simulations.

2.2.12 Radiative transfer calculations

We calculate the radiative forcing (RF) due to individual contrails using the lookup tables provided by Wolf et al. (2023) which embed results from 283,500 simulations with the libRadtran 2.0.1 radiative transfer model (Emde et al., 2016). RF is calculated once per storage time step, as there is not currently any coupling in the simulation between radiative transfer and ice microphysics. To determine the RF, we represent the contrail as a single homogeneous ice cloud. The effective radius of the ice cloud is calculated as the surface area-weighted mean radius of the crystals. The ice cloud temperature is calculated as the number-weighted mean temperature of the clusters; it is assumed that this is a reasonable proxy for the cloud-top temperature as the highest number densities are usually found near the contrail top. The mean ice water content is calculated as the total ice mass in the contrail per unit segment length divided by the area of the contrail hull. The layer depth is taken as simply the difference in altitude between the lowest and highest cluster. Finally the layer width is calculated as the hull area divided by the layer depth. This may overestimate depth and underestimate width, especially for highly sheared contrails.

The lookup table data only represents a single layer thickness of 1,000 m. However, an analysis of sensitivity to layer geometrical depth in Wolf et al. (2023) showed that the effect of differences in layer thickness from 500 to 1,500 m could be accurately captured if interpolation is performed against the ice water path rather than the ice water content, albeit with larger errors in longwave than shortwave radiative forcing. Since the ice water path is equivalent to the layer depth multiplied by the ice water content for a homogeneous layer, this is trivial to calculate for both the CLAMP output and the lookup table data.

Once the CLAMP data has been converted into a representative effective radius, cloud temperature, and ice water path, the local radiative forcing is calculated by looking up the appropriate value in the tables supplied by Wolf et al. (2023) for the current local time (i.e. solar zenith angle) and with user-supplied data for the local surface temperature, liquid cloud water path, and surface albedo. Unless otherwise specified it is assumed that the ice crystals are best represented as aggregates although the data for plates and droxtals are included as part of the CLAMP repository. The local radiative forcing (W m^{-2}) is

https://doi.org/10.5194/egusphere-2026-4489
Preprint. Discussion started: 13 August 2026

converted into an energy forcing (J) through multiplication by the layer width (m), segment length (m – see Section 2.2.7), and diagnostic time step (s).

We also calculate a limited set of diagnostic quantities. The extinction coefficient E is calculated in m^{-1} for each grid cell following the approach described by Unterstrasser and Gierens (2010a), as

$$E = \mathrm{IWC} \times \left(3.448 + \frac{2.431 \times 10^{-3}}{r_{\mathrm{eff}}}\right) \tag{27}$$

where IWC is the local ice water content in kg m^{-3} and r_{eff} is the local crystal effective radius in meters. This quantity is integrated vertically and horizontally to give the horizontal and vertical profiles of optical depth, respectively, while the total extinction is calculated as the 2D integral of E over the entire domain. Layer optical depth is then calculated as the total extinction divided by the layer width calculated previously.

This approach is an approximation only, and does not (for example) consider the presence of other contrails or ice clouds. Implementation of more complex schemes is considered a priority for future research.

3 Model performance

We first demonstrate a reference contrail simulation with CLAMP (Section 3.1), before evaluating the sensitivity of the model to typical input parameters (Section 3.2). We then compare the model results to those in recent literature for canonical test cases (Section 3.3), before finally directly evaluating the effect of addressing the energy budget challenge identified earlier (Section 3.4).

3.1 Reference simulation

To demonstrate typical performance of CLAMP we define a set of reference parameters. Table 1 shows the parameters used to set up the model itself, regardless of the specific details of a given case. These are applied across all simulations described in this manuscript. The lognormal standard deviation in post-vortex crystal mass σ_m is described in Unterstrasser and Sölch (2010), and can be calculated from their width parameter $r_{\mathrm{SD}} = \exp((\ln \sigma_m)^2)$. Our default standard deviation is the result of choosing $r_{\mathrm{SD}} = 3$, consistent with results from a Large Eddy Simulation study of the contrail-to-cirrus transition (Unterstrasser, 2014). Sensitivity of the simulation to some of these parameters is briefly explored in Appendix B.

https://doi.org/10.5194/egusphere-2026-4489
Preprint. Discussion started: 13 August 2026

Table 1. Key model parameters used in CLAMP, and their default values.

Parameter	Default	Description
lognorm_standard_deviation	2.85	Mass standard deviation of the ice crystal population σ_m, unitless
dt_default	600	Outer time step, s
nx_max	1000	Maximum number of cells (horizontal)
minimum_particle_ei	10^{13}	Minimum particle emissions index in the early plume, particles per kg fuel
dx	50	Initial horizontal grid spacing, m
dy	10	Initial vertical grid spacing, m
kelvin_effect	False	Include explicit Kelvin effect after vortex sinking, boolean
yx_scaling	5	Factor used to scale horizontal distances for nearest-neighbor searches, unitless
ode_atol	10^{-6}	Absolute tolerance used during integration for error correction, kg
ode_rtol	10^{-3}	Relative tolerance used during integration for error correction, unitless
ode_solver	RK23	Solver used for ice growth (Runge-Kutta 2nd-order with 3rd-order error correction)
n_clusters	1500	Number of ice clusters to use, unitless

Table 2 shows the parameters passed to the meteorology submodule to define the reference case used throughout this section. These parameters define the relevant vertical profiles (e.g. of temperature and humidity), the application of synoptic-scale updrafts to the domain, and the application of stochastic gravity wave forcing. All simulations in this manuscript represent a stable supersaturated layer, with the only variations in ambient humidity resulting from either a non-zero updraft speed or gravity wave-induced temperature fluctuations (Kärcher and Corcos, 2025; Kärcher and Podglajen, 2023). The Brunt-Väisälä frequency is calculated based on the local temperature lapse rate as $N^2 = \frac{g}{T}\left(\Gamma - \frac{g}{c_p}\right)$. This is used only in the contrail vortex process parameterization (Section 2.2.1) and (if enabled) gravity wave forcing calculations (Section 2.2.10). It is assumed that this will not change over time. The horizontal eddy diffusivity, D_H, is set to 10 m^{2}s^{-1} as a representative value for the upper troposphere (Ueda et al., 2012). A short sensitivity test revealed little sensitivity to this parameter (see Appendix B).

Table 2. Meteorological parameters for the reference simulation. *Parameters are varied between simulations as described. **Used only for calculation of solar zenith angle in radiative forcing estimates. ***Calculated internally from lapse rate.

Parameter	Default	Description
brunt_vaisala***	0.0086	Buoyancy (Brunt-Väisälä) frequency, s^{-1}
layer_depth	1000	Depth of the supersaturated layer, m
layer_rhi	1.1	Relative humidity with respect to ice in the layer, unitless
subsat_rhi	0.50	Relative humidity with respect to ice below the layer, unitless
lapse_rate	-8.14	Rate of change of temperature with altitude, K/km

https://doi.org/10.5194/egusphere-2026-4489
Preprint. Discussion started: 13 August 2026

reference_temperature	217	Temperature at the altitude of contrail formation, K
shear	0.0060	Vertical wind shear $\left(\frac{du}{dz}\right)$ perpendicular to flight direction, m s^{-1} m^{-1}
updraft_cm_s*	0.0	Synoptic-scale updraft speed, cm s^{-1}
horizontal_eddy_diffusivity	10	Horizontal eddy diffusivity D_H, m s^{-2}
latitude	60	Latitude of (0,0) in the domain, degrees North
longitude**	0.0	Longitude of (0,0) in the domain, degrees East
apply_gravity_waves*	False	Include stochastic gravity wave-induced forcing, boolean
gw_mean_fluctuation*	0.10	Mean gravity wave-induced updraft speed $\overline{\omega}$, m s^{-1}
t_init**	-	Date-time (YYYY-MM-DDTHH:MM:SS) of contrail formation

Finally, Table 3 shows the parameters used which are specific to the simulated aircraft. These are mostly derived from the baseline kerosene contrail case in Unterstrasser and Lottermoser (2025) for an Airbus A350/Boeing 777-like aircraft.

Table 3. Aircraft parameters used for the reference simulation. *Sometimes referred to as "overall propulsive efficiency" or "overall efficiency of propulsion" in contrail literature (Bräuer et al., 2021; Schumann, 2000)**, this is the overall efficiency** $\left(\eta_o \simeq \frac{Fu_0}{\dot{m}_f Q}\right)$ **rather than the propulsive efficiency** $\left(\eta_p \simeq \frac{2u_0}{u_e+u_0}\right)$**.**

Parameter	Default	Description
soot_ei	2.8×10^{14}	Soot number emissions index, particles per kg fuel
p_flight	238	Pressure at flight altitude, hPa
flight_velocity	250	Aircraft velocity u_0, m s^{-1}
fuel_rate	3.0	Fuel flow rate summed across all engines $\dot{m}_f$, kg s^{-1}
lower_heating_value	43.2×10^{6}	Fuel lower heating value Q, J kg^{-1}
wing_span	60.9	Aircraft wing span, m
ei_h2o	1.25	Water vapor emissions index, kg H_2O per kg fuel
efficiency	0.3	Engine overall efficiency η_o, unitless*

Simulating the base contrail with this configuration results in a persistent contrail. Over 99% of the soot particles generate an ice crystal during the jet phase but 87% of these sublimate during the vortex sinking process, resulting in 3.4×10^{12} crystals per meter when the mature plume phase simulation begins. The contrail survives for 12 hours before fully sublimating, simulated in an average of 48.3 seconds (median across three samples, range 45.9 to 48.8 seconds) on one core of an Intel Xeon Gold 6348 2.60 GHz machine. Simulations with CLAMP show CPU utilization of 97-99%.

Figure 7 shows how the contrail ice crystal number and total mass evolve over the course of the simulation. This does not include the effect of losses during the vortex phase, as these are accounted for during initialization. The number of ice

https://doi.org/10.5194/egusphere-2026-4489
Preprint. Discussion started: 13 August 2026

crystals per meter remains constant until the lowermost crystals settle out of the supersaturated layer after three hours. Total ice mass of the contrail initially rises monotonically during the same period before plateauing. Whereas the number of ice crystals begins to fall after three hours, total ice mass remains approximately constant for a further four hours before declining towards zero.

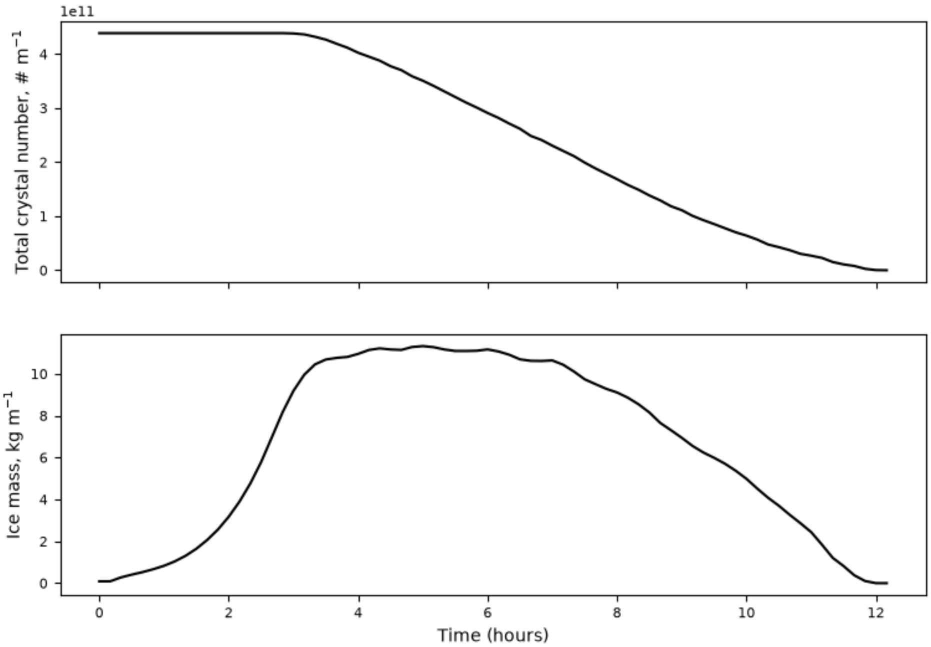

Figure 7. Time series of total crystal number (upper panel) and mass (lower panel) per unit depth of the reference contrail. Time is shown since decay of the vortex system, assumed to take 6 minutes (Lottermoser and Unterstrasser, 2025)**.**

The constant ice crystal number shown during the initial period is consistent with results from Unterstrasser and Gierens (2010a) in which in-situ crystal losses were found to be negligible after the vortex phase and prior to crystals reaching the subsaturated layer. Lewellen et al. (2014) found that this may not be true if the Kelvin effect is included, but in CLAMP most grid cells in the mature plume are assigned uniquely to a single cluster. This limits opportunities for spectral ripening, and therefore for crystal losses. Since crystal loss in CLAMP can occur only when an entire cluster fully sublimates, the number of ice crystals only begins to decrease when a cluster has given up all of its ice mass and yet still finds itself in subsaturated air.

The more complex behavior of the total ice mass can be explained by examining the evolution of the contrail cross section, shown in Figure 8. During the first three hours, water vapor uptake takes place over a growing area. The combination of accelerating settling speeds and constant vertical wind shear result in non-linear growth in the contrail's cross-sectional area, and thus in the total water vapor available for uptake. This pattern has been consistently observed in LES studies of long-

https://doi.org/10.5194/egusphere-2026-4489
Preprint. Discussion started: 13 August 2026

term contrail behavior in a stable, supersaturated layer (Lewellen et al., 2014; Lewellen, 2014; Unterstrasser and Gierens, 2010a, b).

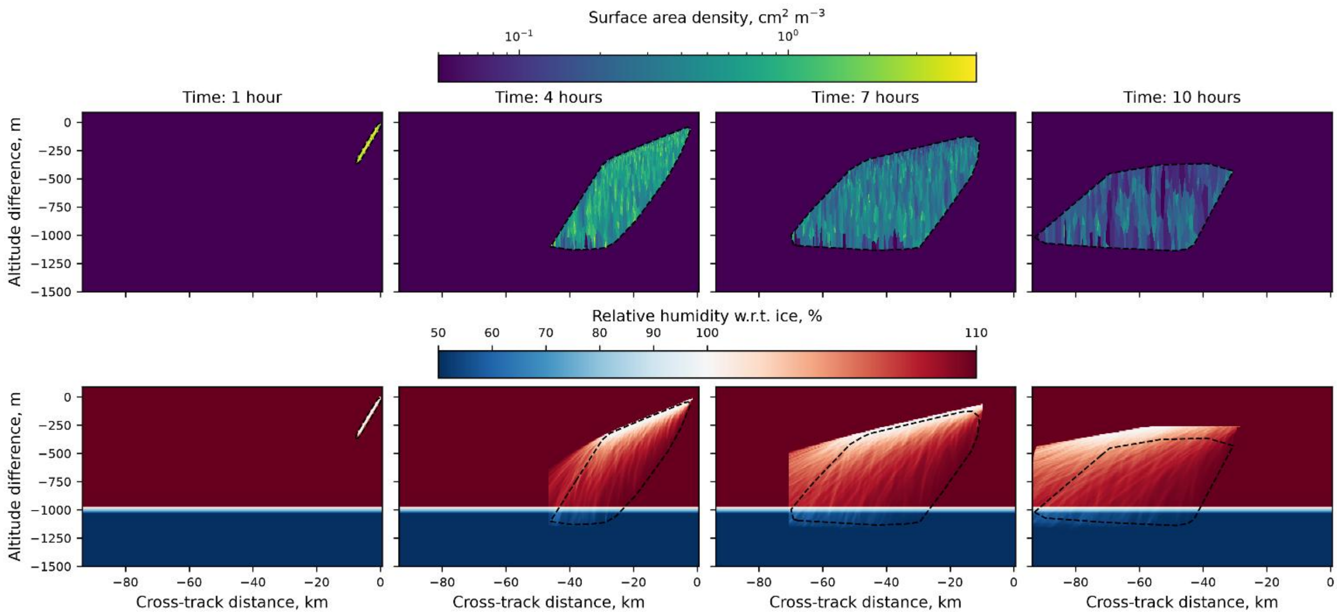

Figure 8. Contrail cross section 1, 4, 7, and 10 hours after decay of the vortex system. The upper row shows the surface area density, while the lower row shows the ambient relative humidity with respect to ice. Dashed lines indicate the hull of the contrail ice crystals at each time step.

After three hours, clusters have settled into the subsaturated region and begin to give up water vapor. This is a gradual process, limited by both the rate of ice sublimation and the degree of local subsaturation. Since the layer is at only 50% relative humidity with respect to ice, the falling clusters do not have sufficient water to bring the air to saturation. However, as the ice crystals sublimate they are exposed to air which is less subsaturated, while their reduction in mass also means a reduction in fall speed. This means that loss of ice mass is gradual, with ice loss below the supersaturated layer approximately balanced by uptake of water as higher-altitude crystals descend into fresh air exposed by shear. The rate-limited nature of water exchange is demonstrated by the presence of areas within the contrail hull with relative humidities ranging from 50-110% even after four hours of simulation.

This behavior is driven by the ability of CLAMP to capture ice crystal gravitational sorting. Figure 9 shows how the fall velocity and center of mass location evolve over time. During the first three hours, the mass-weighted mean crystal fall velocity closely tracks the rate of descent of the center of mass, reproducing the "ballistic" trajectory of zero-dimensional models as discussed by Akhtar Martínez et al. (2025). The mean, median, and 5th and 95th percentiles of the vertical mass distribution follow similar trajectories during this period.

https://doi.org/10.5194/egusphere-2026-4489
Preprint. Discussion started: 13 August 2026

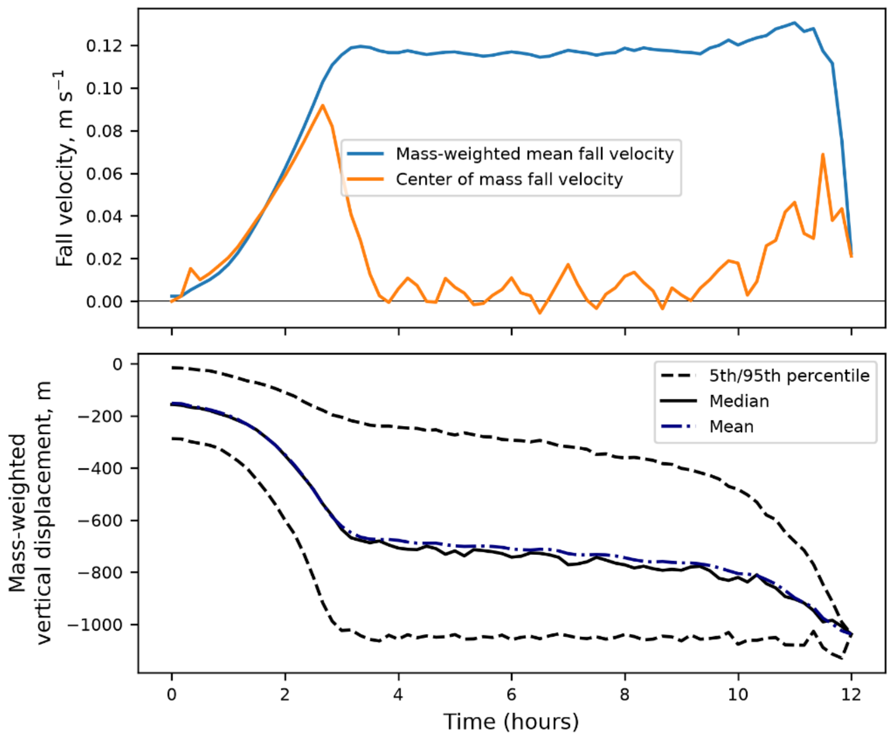

830 **Figure 9. Metrics of contrail descent over time. Upper panel: fall velocity calculated as either the mass-weighted mean fall velocity (blue) or the rate of descent of the contrail center of mass (orange). Lower panel: vertical distribution of mass over time. Dashed lines show the mass-weighted 5th and 95th percentiles of location, with the median shown as a solid black line. The mass-weighted mean is shown as a dash-dotted blue line.**

However, once the lowermost crystals reach the subsaturated layer the two velocities diverge. Within this second regime, the lower boundary of the contrail is stationary while the upper boundary and center of mass slowly descend.

3.2 Sensitivity to input parameters

We explore sensitivity of total ice mass, number of ice crystals, and integrated total extinction to variation in the soot emissions index (Section 3.2.1), variation in meteorological parameters (Section 3.2.2), and inclusion of stochastic gravity wave forcing (Section 3.2.3). Unless otherwise specified all input parameters are as specified in Table 2 and Table 3 for a stable supersaturated layer. We perform three simulations of each configuration and take the average to account for the effect of random variability, with the exception of simulations in Section 3.2.3 with non-zero gravity wave forcing for which we perform 50 simulations. For all simulations we show total ice mass, number of ice crystals, and cumulative energy forcing per meter of contrail formed. Energy forcing is calculated assuming a formation time of 12:00 UTC on July 1st 2019, at a latitude of 60° N and longitude of 0°. Advection of the contrail is neglected for this calculation, and radiative forcing is calculated assuming a surface albedo of 0.3, a surface temperature of 280 K, and no underlying liquid water clouds. Across

https://doi.org/10.5194/egusphere-2026-4489
Preprint. Discussion started: 13 August 2026

all 216 simulations in this section and using the same hardware as in Section 3.1, the median simulation completes in 40.1 seconds, ranging from a minimum of 11.4 to a maximum of 120 seconds.

3.2.1 Sensitivity to soot emissions index

Figure 10 shows how results from CLAMP vary as a function of the soot emissions index, with the caveat that "soot" in this case may more accurately be considered a combination of early non-volatile and volatile particulate matter (Voigt et al., 2026). The default case of 2.8×10^{14} particles per kg of fuel burned is shown in black, alongside two cases where the emissions index is reduced by a factor of 10 (orange) or 100 (blue).

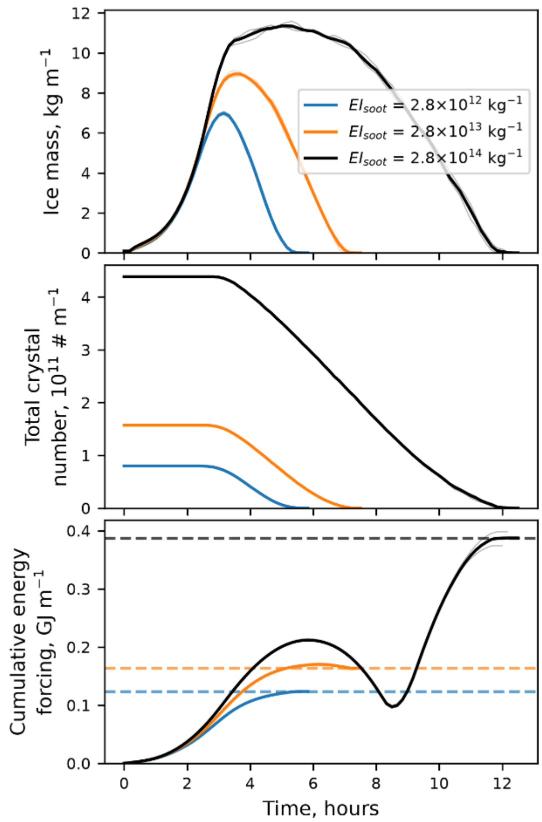

Figure 10. Evolution of a contrail with different soot emissions indices. Panels show ice mass (top), total crystal number (middle), and cumulative energy forcing (bottom) for simulations as a function of time since vortex decay (six minutes after aircraft passage). Thin lines indicate individual simulations, with the average over three realizations shown as a thick line. Dashed lines show the cumulative energy forcing at completion of the simulation.

Our baseline case results in a net energy forcing of 0.387 GJ m^{-1}. Although only a single case, the order of magnitude is consistent with the global mean of 0.331 GJ m^{-1} calculated using CoCiP for flights in 2019 (Teoh et al., 2024a). Variability due to random factors in the simulation has a negligible effect on the simulation, as indicated by the relatively small differences between individual realizations.

https://doi.org/10.5194/egusphere-2026-4489
Preprint. Discussion started: 13 August 2026

Consistent with other studies of the effect of soot emissions index, we find that reducing the emissions index also produces a sublinear reduction in the anticipated climate impact. Integrated ice surface area provides a proxy for climate impact, on the basis that both shortwave and longwave radiative forcing are expected to vary as a function of this quantity. Reducing the soot emissions index (EI_{soot}) by a factor of 10 results in a 64% reduction in integrated surface area, while a factor 100 reduction in EI_{soot} yields an 82% reduction in the same metric. This closely follows the reduction in initial crystal number, reflecting the near-linear relationship observed by prior studies between initial crystal number and lifetime integrated extinction in the particle-rich regime (Bier and Burkhardt, 2022; Lottermoser and Unterstrasser, 2026; Märkl et al., 2024; Rubin-Zuzic et al., 2025). The non-linear relationship between soot emissions index and initial crystal number is partially due to the enforcement of a minimum particle emissions index of 10^{13} kg^{-1}, and partially due to the non-linear relationship between pre-vortex and post-vortex crystal number represented by the vortex sinking parameterization (Lottermoser and Unterstrasser, 2025).

The net energy forcing also falls non-linearly, with a 10 and 100 times reduction in EI_{soot} resulting in reductions of 58% and 68% respectively in energy forcing. This is only for a single case, and does not necessarily reflect the change in climate impact anticipated for fleet-wide reductions in soot emissions. However Figure 10 illustrates the degree of non-linearity hidden by this response, as two effects compete. Reducing the soot emissions index reduces lifetime, as crystals are on average larger and settle more quickly such that the reduced EI cases sublimate within seven hours. However, the radiative forcing of the contrail is strongly negative between 6.5 and 8.5 hours (18:30 – 20:30 local time) due to the high solar zenith angle (Myhre et al., 2009), resulting in a sharp reduction in contrail energy forcing. Had the contrail sublimated at this point, it would have had a lower energy forcing than the cases with a lower soot emissions index. This shows the sensitivity of contrail energy forcing to the time, season, and location of the flight as well as to other factors which may cause the contrail to sublimate earlier (Hofer and Gierens, 2025).

3.2.2 Sensitivity to meteorological parameters

Figure 11 shows how the same metrics change with variation in common meteorological parameters. Across all panels, results for the reference case are shown in black with sensitivity cases shown in blue and orange.

The simplest response is to changes in the supersaturated layer depth. As the layer depth increases from 1,000 to 1,500 m, the peak ice mass increases from 11 to 21 kg/m, with an associated 55% increase in the integrated surface area. Conversely, a reduction from 1,000 to 500 m depth reduces the peak mass to 3.8 kg/m and the integrated surface area by 57%. However these changes are not reflected in the lifetime of the contrail. Although the lowermost contrail crystals do reach the subsaturated layer more quickly, differences in timing are small as shown by the small differences (less than one hour) in onset of crystal loss. This is due to the non-linear increase in fall speed of the lowermost crystals in the precipitation plume.

https://doi.org/10.5194/egusphere-2026-4489
Preprint. Discussion started: 13 August 2026

Meanwhile the uppermost crystals are also accelerating and are increasingly exposed to humid air due to the continuing effects of wind shear. Nonetheless, the contrails forming in thicker layers are able to achieve greater widths, as the larger vertical extent of the contrail allows wind shear to spread the particles over a greater horizontal distance. The 64% increase (65% decrease) in energy forcing associated with a thicker (thinner) layer is therefore driven more by the change in mass and width of the contrail, rather than any effect on lifetime.

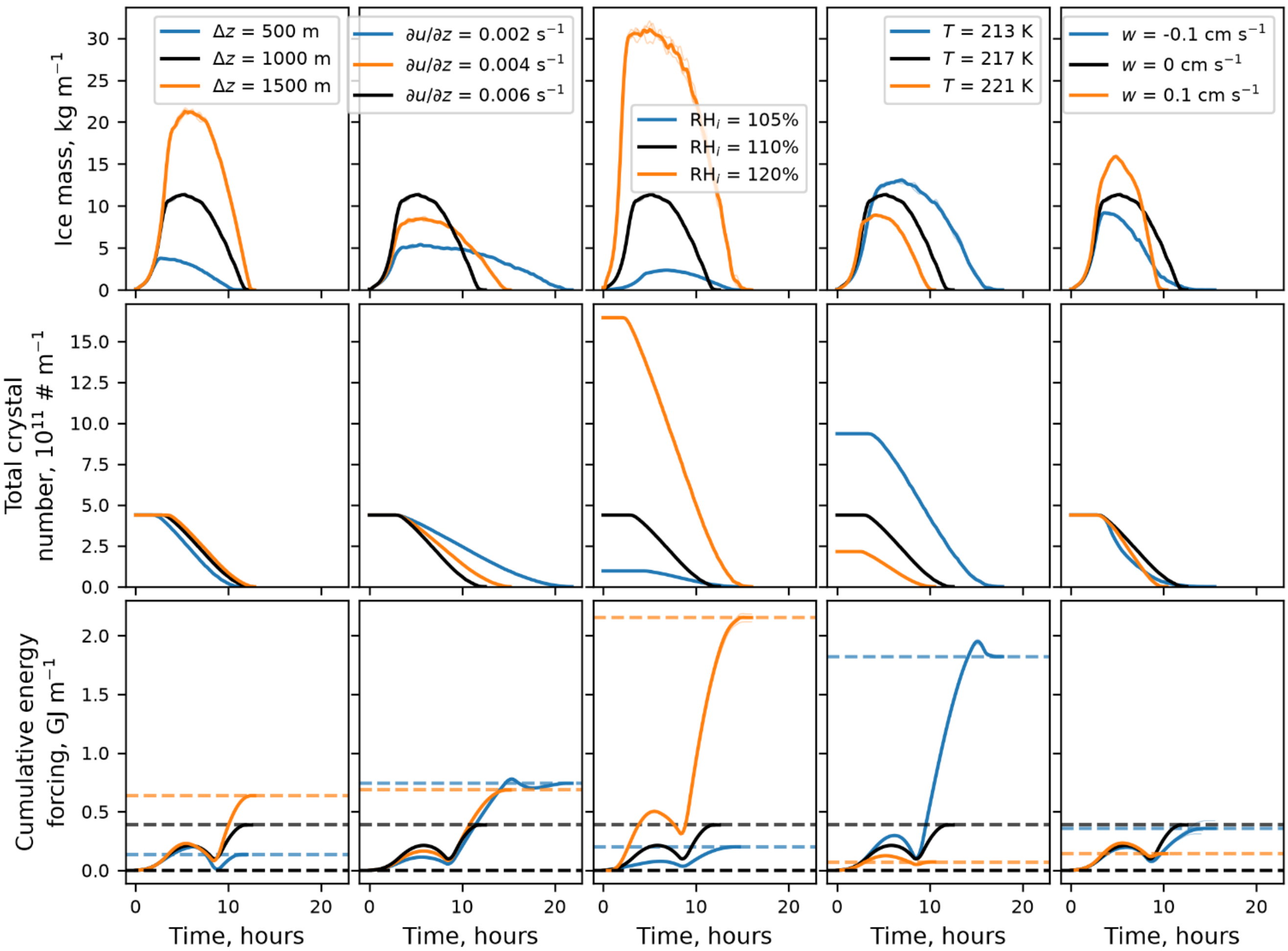

Figure 11. Evolution of a contrail with different meteorological parameters. Rows are as shown in Figure 10. From left to right, columns show sensitivity to supersaturated layer depth (Δ*z*), wind shear (∂u/∂z), layer relative humidity with respect to ice (RH$_i$), temperature (*T*), and updraft velocity (*w*). Negative updraft velocities correspond to a downwards (warming) synoptic scale motion. Black lines show the same simulation across all panels.

Changes in climate impact due to changes in wind shear are instead dominated by changes in lifetime. Reducing the wind shear means that the uppermost crystals are less quickly exposed to fresh (humid) air, instead spending longer settling through air which has already been depleted by earlier ice crystals. Since the lower wind shear essentially slows down the contrail's evolution, decreasing the wind shear from 6 m s^{-1} km^{-1} to 2 m s^{-1} km^{-1} reduces the lifetime integrated surface area

https://doi.org/10.5194/egusphere-2026-4489
Preprint. Discussion started: 13 August 2026

by 1.2%. However it increases the energy forcing by 92%. This is largely due to the timing of the change, as the lower wind shear case persists further into the nighttime despite having a peak width 41% lower.

Changing the relative humidity and temperature both have mixed effects, as these parameters affect both the vortex sinking parameterization and the behavior of the diffusion phase modelled explicitly by CLAMP. Increasing RH_i results in a monotonic increase in initial ice crystal count, integrated surface area, peak ice mass, and energy forcing. Lifetime of the contrail is dictated by competition between an increase in ice crystal number, which tends to extend lifetimes by producing smaller crystals, and the increase in available water vapor, which has the opposite effect. Decreasing the temperature instead causes a monotonic increase in all of these quantities, as it both increases the initial ice crystal count and decreases the available water vapor (for a fixed value of RH_i).

In comparison to these, the imposition of an updraft or downdraft has a complex effect. A constant updraft of 0.1 cm/s decreases the temperature, increasing the availability of water and therefore increasing sedimentation speeds. This results in in 1.7% increase in integrated surface area but a 63% decrease in energy forcing, as the contrail sublimates before the onset of nighttime. An equal-speed downdraft has the opposite effect, reducing ice mass and therefore sedimentation speed but also driving the contrail towards sublimation. Nonetheless, despite a 29% reduction in integrated surface area we find only a 7.7% decrease in energy forcing relative to the reference case. This again shows the sensitivity of the contrail forcing to the precise timing and circumstances of its formation, and not just its physical characteristics.

3.2.3 The effect of gravity wave forcing

Finally we examine the influence of uncertain gravity wave forcing. Figure 12 shows how a mean gravity wave forcing of up to 0.10 m s^{-1} affects evolution of the contrail. For these simulations we average over a larger set of 50 simulations due to the stochastic nature of the gravity wave parameterization (Kärcher and Corcos, 2025; Kärcher and Podglajen, 2023).

https://doi.org/10.5194/egusphere-2026-4489
Preprint. Discussion started: 13 August 2026

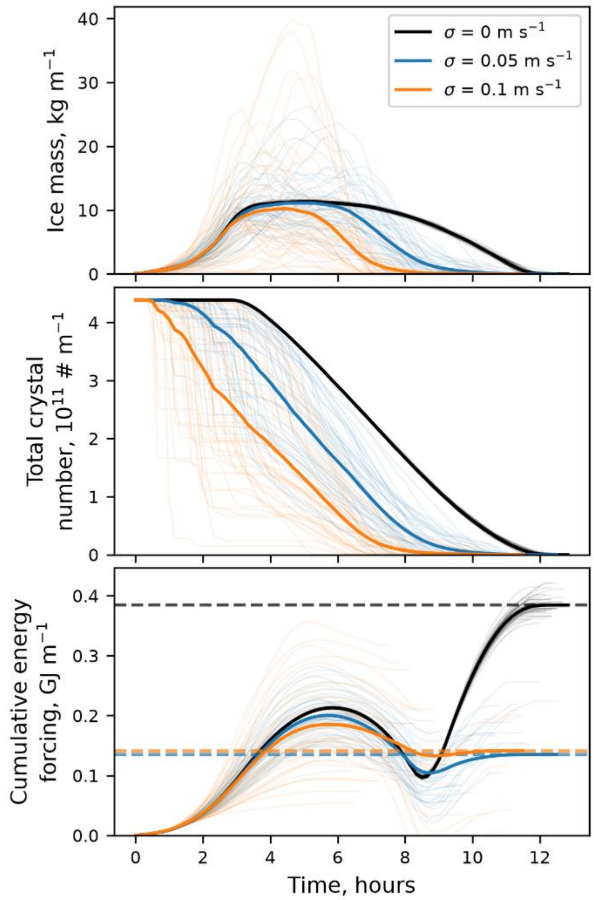

Figure 12. Evolution of a contrail with different mean gravity wave forcing. Rows are as shown in Figure 10. Thick lines here indicate an average over 50 simulations.

We find that inclusion of a gravity wave forcing term significantly changes the behavior of the simulation. First, variability between simulations increases dramatically. Without gravity wave forcing, variations between runs are driven only by the random initial placement of contrail clusters. This results in a peak ice mass value of 11.3 kg m^{-1} and an interquartile range (relative to the mean) of 2.1%. This peak is reduced to 10.3 kg m^{-1} for σ = 0.1 m s^{-1}, but the interquartile range increases to 88%. Second, as the gravity wave forcing increases so too does the ice crystal loss rate. This occurs because brief downward motions heat the contrail, causing clusters carrying the smallest crystals to sublimate. Even though, on average, the air mass will then rise and the water will be taken up by surviving crystals, this nonetheless results in an overall reduction in crystal number and an increase in the mean crystal radius. The contrail's lifetime is thus shortened by both the possibility of prolonged adiabatic heating causing complete sublimation, and the effect of intermittent heating resulting in larger crystals and faster settling. In this specific simulation the introduction of gravity wave forcing results in a 63-65% reduction in cumulative energy forcing, as the longer-lived case (with no gravity wave forcing) persists into nighttime.

https://doi.org/10.5194/egusphere-2026-4489
Preprint. Discussion started: 13 August 2026

Previous contrail models have attempted to capture this effect through parameterizations. In CoCiP, for example, a constant rate of ice crystal loss is assumed due to gravity wave forcing (Schumann, 2012). The CoCiP parameterization, which scales with the Brunt-Väisälä frequency, temperature lapse rate, and vertical velocity fluctuations would in theory allow calculations to be performed which capture the effect of gravity wave-driven vertical velocity fluctuations without needing ensemble simulations. However the behavior shown in Figure 12 does not follow this pattern; rather than the rate of crystal loss being dictated by the fluctuation rate, increasing the gravity wave fluctuation velocity instead results in earlier onset of crystal losses when considering the average case but no change in the loss rate once this process begins. Further work is needed to identify an efficient approach which can accurately capture the effect of gravity waves without needing ensemble simulations.

3.3 Comparison to literature results

Thus far all results have only shown CLAMP output, with no reference to other models or to observations. Given that CLAMP's focus is on the long-term evolution of contrails, which remains difficult to directly observe, we focus here on comparing results from CLAMP for canonical simulations against those from other models of the long-term behavior of contrails.

Akhtar Martínez et al. (2025) explored how two such models, the Contrail Cirrus Prediction model (CoCiP: Schumann, 2012) and the Aircraft Plume Chemistry, Emissions, and Microphysics Model (APCEMM: Fritz et al., 2020) simulate contrails under different meteorological conditions.

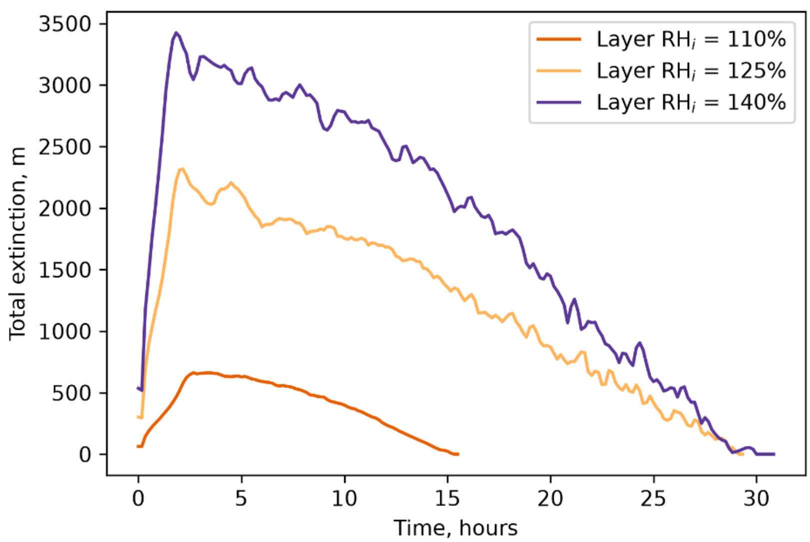

Figure 13. Total extinction over time for three different layer relative humidities. Colors and cases are identical to those shown in Figure 8 of Akhtar Martínez et al. (2025).

Figure 13 shows total extinction over time from CLAMP for the same three cases as were given in Figure 8 of Akhtar Martínez et al. (2025), demonstrating the effect of layer relative humidity on contrail evolution. At the lowest relative humidity (110%), extinction grows for two hours before peaking at 660 m. It then falls slowly, with the contrail fully sublimating after approximately 16 hours. This is similar to the behavior exhibited by APCEMM, which showed growth for approximately 2.5 hours to a maximum value of 1000 m before gradually falling to zero by roughly 12.5 hours. Similarly CLAMP shows non-linear increases in extinction with increasing RH_i, with the peak value increasing to 2300 and then 3400 m as RH_i increases to 125 and 140% respectively; APCEMM shows growth to 2000 and then 2800 m for the same cases. APCEMM also found only modest changes in contrail lifetime with the contrail sublimating after 14 hours for even the highest RH_i case. CLAMP shows a large increase in contrail lifetime between the 110 and 125% cases, but as with APCEMM shows little difference between the 125 and 140% case. This is because of two competing factors: the higher RH_i increases the number of crystals which survive the vortex phase, but also results in more water uptake to those crystals and therefore faster settling of the primary wake. Although the results are qualitatively similar to the results from APCEMM, the sensitivity of CLAMP to RH_i is greater in terms of both peak extinction and contrail lifetime. We speculate that this difference is in part due to differences in the early plume parameterizations but also due to CLAMP's tendency to preserve a large population of small crystals in the primary wake, allowing the contrail to last longer than is the case when simulated by APCEMM.

We furthermore compare CLAMP's results to those from a sensitivity study conducted in Akhtar Martínez et al. (2025) which evaluates the consequences of varying layer depth, the relative humidities in the subsaturated and supersaturated areas of the domain, the temperature at cruise altitude, and the overall wind shear. Results are shown in Figure 14 against results from the APCEMM (Fritz et al., 2020) and CoCiP (Engberg et al., 2025; Schumann, 2012) models, as simulated in the original study. However all CLAMP simulations are allowed to continue for up to 72 hours, whereas simulations in Akhtar Martínez et al. (2025) were limited to 24 hours.

https://doi.org/10.5194/egusphere-2026-4489
Preprint. Discussion started: 13 August 2026

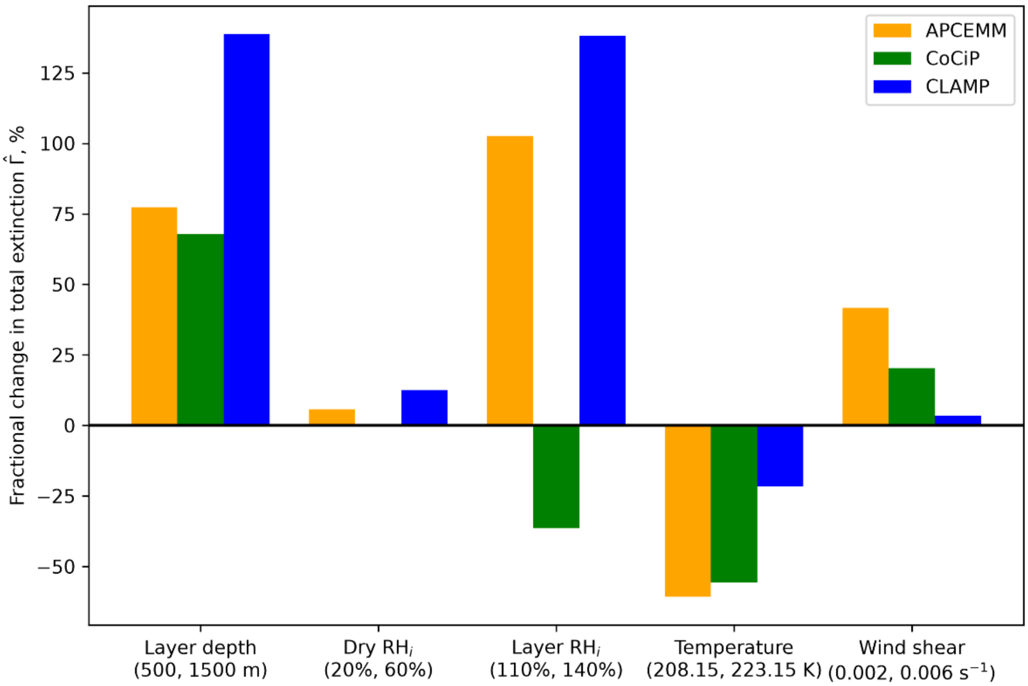

Figure 14. Sensitivity of lifetime integrated total extinction to variation in meteorological parameters, following the protocol described in Akhtar Martínez et al. (2025)**. Data for APCEMM and CoCiP are taken from their Appendix D. CLAMP simulations are allowed to continue until sublimation of the entire contrail.**

CLAMP agrees directionally with APCEMM across all five variables, and the ranked order of effect size is similar: increases in layer relative humidity and depth have the largest (positive) effect, while increasing temperature causes a reduction in overall extinction. This latter effect reverses however if only the first 24 hours are considered, as at 208 K 45% of the contrail total extinction occurs after 24 hours. While APCEMM and CLAMP both agree that the changes in subsaturated region ("dry") relative humidity and wind shear have smaller effects, CLAMP finds that increasing wind shear has almost zero impact where APCEMM finds a 42% increase. This is due to the behavior previously discussed and shown in Figure 11, where increasing wind shear results in faster ice mass uptake but also faster settling.

Finally, Figure 15 shows the results of reproducing a study from Lottermoser and Unterstrasser (2026). They used the EULAG-LCM large eddy simulation model to simulate five contrails in which the number of ice crystals present prior to vortex phase losses (N_{00}) is prescribed at values ranging from 3.38×10^{10} to 3.38×10^{15} crystals per meter of flight distance. Meteorological and aircraft parameters are chosen to match the original study, including a weak (1 cm/s) updraft which is halted after five hours.

https://doi.org/10.5194/egusphere-2026-4489
Preprint. Discussion started: 13 August 2026

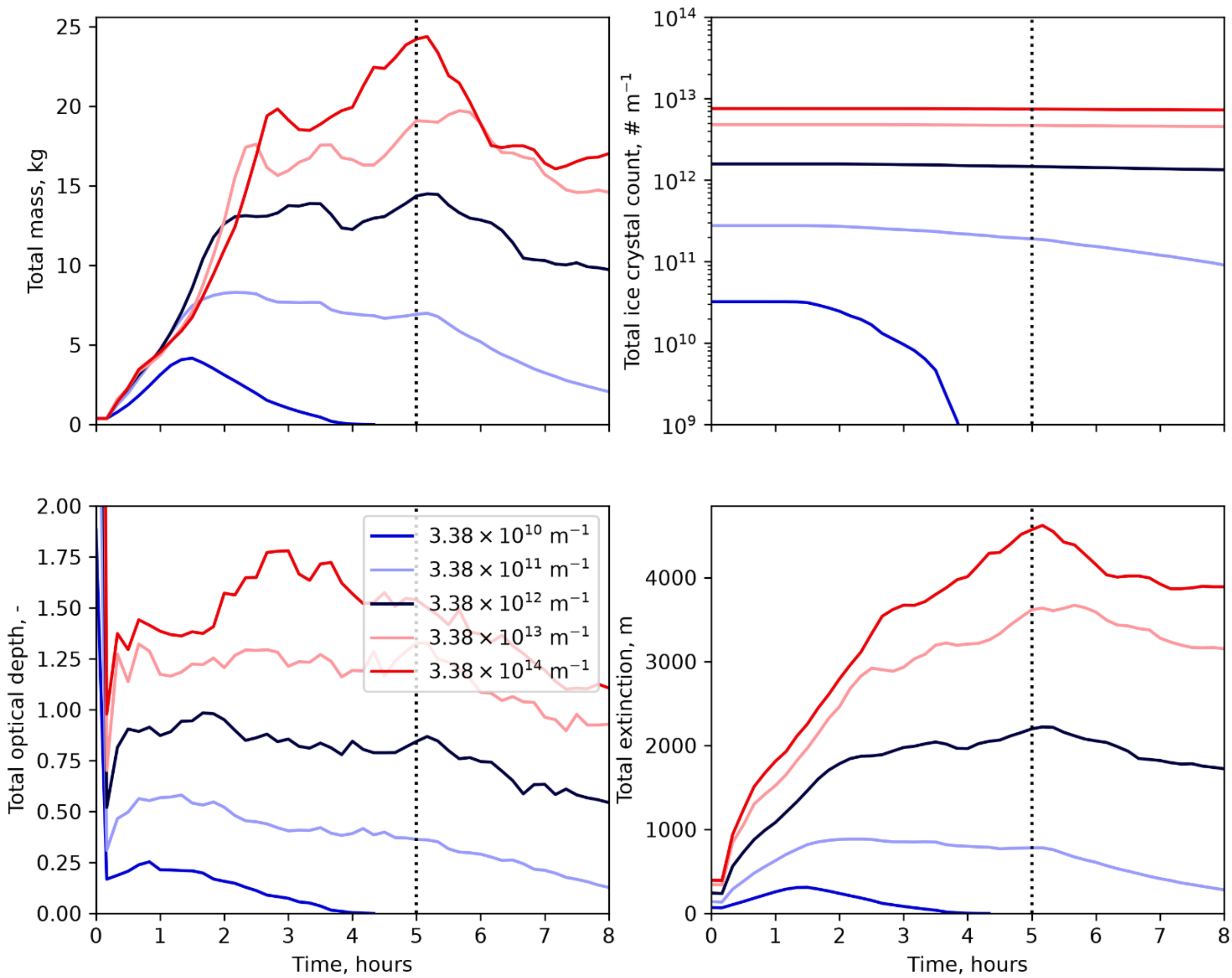

Figure 15. Sensitivity of contrail properties to the total number of crystals formed in the early jet. Upper left: total ice mass per meter of contrail length. Upper right: total number of ice crystals remaining per meter of contrail length. Lower left: mean optical depth. Lower right: total extinction. The vertical dashed line shows the point at which the updraft velocity is reduced from 1 to 0 cm/s. Colours are chosen to match Figure 5 of Lottermoser and Unterstrasser (2026)**.**

CLAMP reproduces the overall trend across the five cases, with increasing ice crystal number resulting in increasing ice mass, optical depth, and total extinction. We similarly find that the case with the smallest value of N_{00} sublimates within approximately four hours, whereas all other cases survive past at least eight hours. The simulated extinction also closely matches that shown in Figure 5 of Lottermoser and Unterstrasser (2026) in both trend and magnitude.

The magnitude of the correspondence is less strong for ice mass and optical depth. The total ice mass in our simulation is consistently roughly half of that found in the original study, and the optical depth is four to six times higher. We hypothesize that this is the result of the contrail spreading too slowly horizontally, resulting in too little uptake of ice mass and thus the

https://doi.org/10.5194/egusphere-2026-4489
Preprint. Discussion started: 13 August 2026

contrail remaining both narrow and optically thick. Differences may also be partially driven by our definition of optical depth, which relies on calculating an effective layer width (see Section 2.2.12), whereas Lottermoser and Unterstrasser instead take the average of all columns where the optical depth exceeds 0.005.

A driving difference between CLAMP and EULAG-LCM is the representation of ice crystal losses. Although we use the same reference data for losses in the vortex sinking phase, the only mechanism by which the ice crystal number in CLAMP can subsequently fall is through sublimation of an entire cluster. For the cases simulated above, where there is no synoptic-scale downdraft or gravity wave forcing, sublimation therefore occurs exclusively through sedimentation. Lottermoser and Unterstrasser's simulations showed that, while sedimentation losses are dominant in EULAG-LCM for lower values of N_{00}, at values of 10^{12} m^{-1} and greater in-situ losses caused sublimation of 41 to 87% of all emitted crystals within eight hours. This explains why agreement between CLAMP and EULAG-LCM is strongest for values of N_{00} below 10^{12} m^{-1}.

3.4 Closure of the thermodynamic budget

As discussed in Section 1.1, CLAMP seeks to address a standing problem which occurs when contrails are represented using Lagrangian trajectories through gridded meteorological output from an Eulerian model. Specifically, models which force the contrail temperature to track that from the grid-scale model do not close their energy budgets. It is impossible to know whether the change in temperature of the parent, Eulerian grid cell is due to e.g. adiabatic cooling (which should change the temperature within the contrail immediately) or grid-scale mixing (which should affect only the air with which the contrail is mixing). CLAMP instead uses a closed energy budget. Temperature changes due to (e.g.) adiabatic cooling directly modify the contrail temperature, whereas changes in the ambient conditions of air with which the contrail is mixing are represented as changes in the relative humidity at the domain boundary (see Sections 2.1.2 and 2.2.4 which discuss the theory and implementation, respectively).

To demonstrate the effect of this representation, we conduct a sensitivity test with time-varying ambient conditions. In this test, the initial conditions are identical to those in the reference case (Section 3.1). However, rather than keeping conditions constant over time, we prescribe a gradual, uniform increase in temperature over the entire domain, assumed for the purposes of this demonstration to be due to grid-scale mixing of air. By linearly increasing the temperature by 1.1 K over three hours we force the ambient relative humidity to drop from 110% to 95.4% at cruise altitude, crossing 100% at exactly two hours. Since this change is not driven by vertical motions, it is represented in CLAMP as a change in the relative humidity at the boundary conditions only and therefore affects the contrail only by dehydrating the air which is brought below the contrail by wind shear. The advected air mass carrying the contrail retains its high relative humidity resulting in a contrail with a peak ice mass of 7.1 kg m^{-1} (Figure 16). Meanwhile that the air brought underneath the contrail by shear becomes marginally subsaturated, meaning that the contrail does not fully sublimate for 22 hours and 20 minutes and remains visible for 4 hours and 50 minutes based on an optical depth threshold for sub-visible cirrus of 0.05 (Frömming et al., 2011; Li et al., 2023).

https://doi.org/10.5194/egusphere-2026-4489
Preprint. Discussion started: 13 August 2026

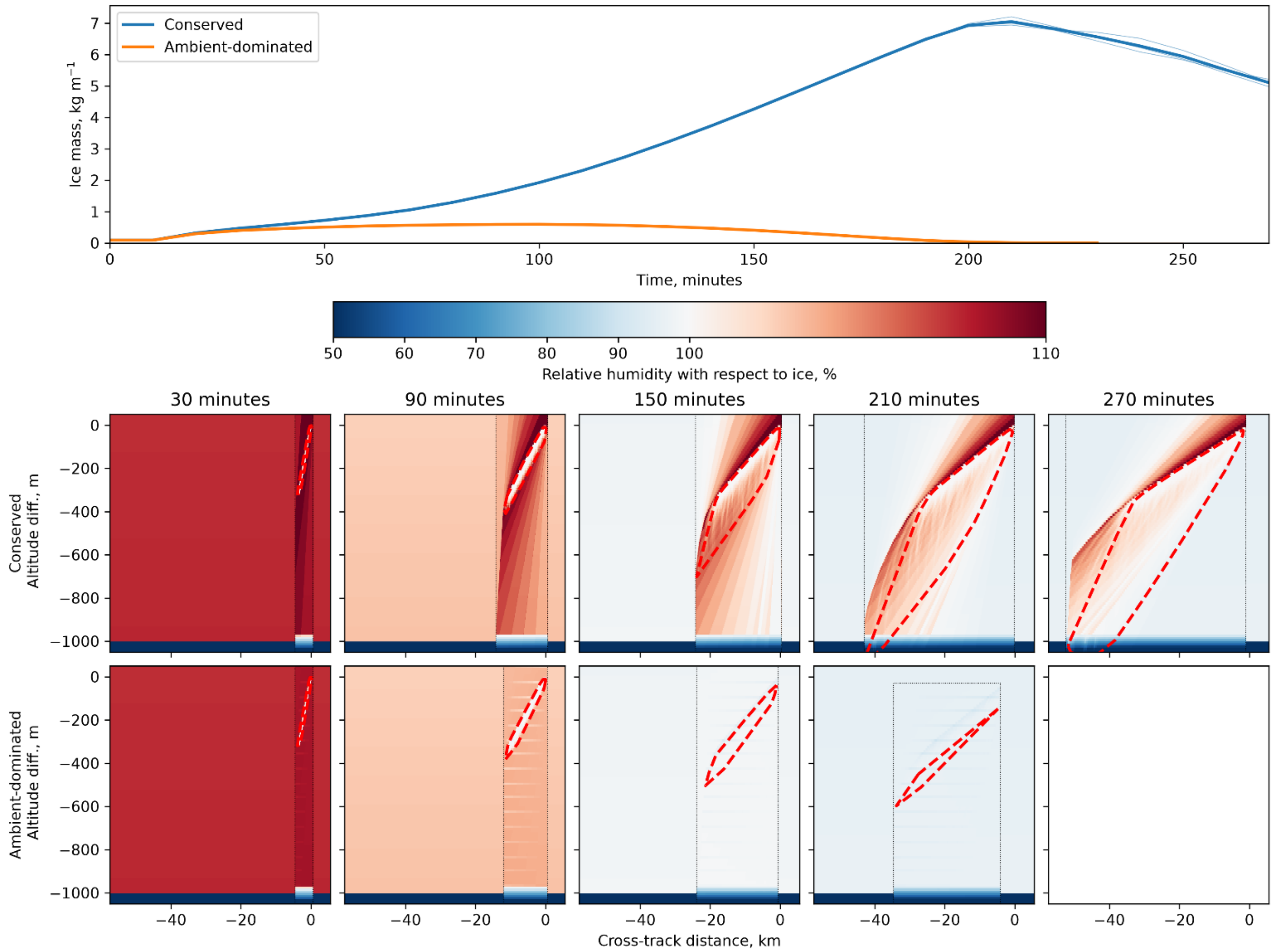

Figure 16. Sensitivity simulation to demonstrate the effect of thermodynamic inconsistency. Results from two simulations are shown: "consistent" uses CLAMP's default approach to representing changes in ambient temperature and humidity, while the "ambient-dominated" case forces temperature in the contrail to track those drawn from the parent model. Upper panel: ice mass over time for each of the two cases, truncated to 270 minutes. Lower ten panels: relative humidity in the contrail cross section. Red dashed lines indicate the hull of the contrail ice crystals at each time step. Dotted black lines indicate the boundary of the domain simulated in CLAMP, with the region outside filled with data based on the current ambient meteorology. The upper row shows results from the "constrained" (CLAMP default) case, while the lower row shows results from the "ambient-dominated" case. Each column shows results one hour apart, starting from 30 minutes (left-most) and ending at 270 minutes (right-most). The humidity fans result from discretization of the meteorological data into five minute increments.

If however the temperature within the contrail is forced to follow that of the ambient meteorology, the contrail rapidly begins to sublimate. Although development is nearly identical during the initial 30 minutes, growth of the contrail ceases within an hour with a peak ice mass of 0.60 kg m^{-1} despite the ambient relative humidity being above 100%. This is for two reasons. First, the air below the contrail is being artificially heated, reducing the amount of water available for contrail growth compared to the standard case. Second, the air within the contrail is being forced below saturation by the same process, causing the crystals to give up water. The continued warming of the contrail means that it full sublimates within 4 hours and 3 minutes, and becomes subvisible within 1 hour and 50 minutes.

This is of course a contrived example, and does not necessarily reflect a real case. However, it does illustrate the need to explicitly separate the sources of changes in meteorological conditions. By isolating the sources of change and maintaining a closed energy budget, CLAMP ensures interpretability of the result while avoiding the risk that different mechanisms of energy or mass transfer are inappropriately transposed.

4 Discussion and conclusions

The Contrail Layer Approximation using Multi-crystal Particles (CLAMP) v1.0 provides an efficient new method of simulating contrail cross-sections, reproducing results from higher-resolution models at a fraction of the cost. By explicitly simulating the 2D cross-section with rate-limited ice microphysics, CLAMP captures the key phenomena limiting water uptake throughout a contrail's lifetime. Meanwhile, by carefully separating the mechanisms by which changes in ambient conditions can influence air within the contrail, CLAMP minimizes the entangled issues of open energy budgets ("thermodynamic inconsistency") and mismatch between the Eulerian and Lagrangian perspectives.

There are several immediate opportunities to improve CLAMP. The assumption that a contrail can be represented by a convex hull means that more complicated meteorological situations, such as a reversal in wind shear, will result in abrupt and non-physical changes in simulated contrail ice mass. Similarly, the exclusive assignment of water vapor to the nearest cluster results in unrealistic sharp gradients in crystal properties across the contrail. Strategies such as the use of a concave hull (e.g. an alpha shape) or using inverse distance weighting to determine the relationship between grid cells and clusters may help to mitigate this shortcoming. It may also be possible to replace the numerical integration of water exchange with an analytical solution.

Crystal losses in CLAMP are likely underestimated, due to the lack of any explicit mechanisms for crystal loss prior to total sublimation of entire clusters. This is likely exacerbated by the relative lack of competition for water between clusters, due to the exclusive cell assignment strategy. In addition to using non-exclusive assignment strategies, it may be necessary to explicitly include parameterizations for in-situ crystal losses. Relaxing the assumption of a monodisperse size distribution for each cluster may also help, even if only by forcing partial sublimation of a cluster to result in some reduction in that cluster's crystal count.

CLAMP's use of a closed energy budget brings some additional challenges. Temperature changes in the host model may be due to factors such as radiative cooling or latent heat release, which should be accounted for in the CLAMP energy budget

https://doi.org/10.5194/egusphere-2026-4489
Preprint. Discussion started: 13 August 2026

but are currently neglected. These factors may be particularly important when vertical motion is tightly coupled to diabatic processes, as is the case in the tropical free troposphere (Sobel et al., 2001) and some extratropical weather systems (Nie and Sobel, 2016). In the case of latent heat release and radiative absorption, both of which affect contrail evolution (Paoli et al., 2017), the same limitation applies for the CoCiP and APCEMM models (Fritz et al., 2020; Schumann, 2012). Implementation of radiative cooling would likely be straightforward, but addressing latent heat release appropriately may require temperatures to be resolved in 2D across the domain. Finally, CLAMP treats the local atmosphere as laminar, with no grid- or sub-grid-scale turbulent fluctuations in velocity or temperature. These fluctuations have previously been shown to significantly accelerate crystal loss in the early plume (Lewellen et al., 2014), but there is no obvious mechanism by which to simulate the effect of these fluctuations without increasing the computational complexity of the simulation.

Despite these limitations, CLAMP provides a new, intermediate-fidelity option for contrail simulations at lower computational cost than models such as APCEMM but with the ability to represent internal heterogeneity which cannot be captured by zero-dimensional models like CoCiP. By using separate treatments for adiabatic heating compared to mixing-in of varying ambient air, it also provides an interpretable and thermodynamically-consistent model for use with archived meteorological data. This makes it ideal for evaluation against large observational datasets of long-term contrail-cirrus evolution at scales beyond those viable for computationally-expensive large eddy simulation models.

Given the difficulty of establishing such datasets, however, a clear next step is to perform at-scale evaluations of contrail models with harmonized inputs. Efforts such as the Coupled Model Intercomparison Project (CMIP) have been transformative in evaluating the degree of consensus between models, as well as providing a benchmark for lower-fidelity models to compare against in the absence of accurate, real-world observations. A contrail model intercomparison project could similarly provide an unbiased assessment of contrail model consensus even before large datasets of aged contrail observations are available, and thus guide future developments in contrail model simulation.

Appendix A: Approximations used for atmospheric quantities

Several of the critical quantities used in CLAMP are impractical or impossible to compute directly, and must therefore be approximated. The formulae used for these quantities in our implementation of CLAMP are listed below. Temperature T is in Kelvin in all cases.

We compute the saturation vapor pressure of water with respect to ice using the recommendation from the World Meteorological Organization (WMO)'s Guide to Instruments (2023 edition), converted to accept temperature in Kelvin rather than Celsius. This is expressed in Pa as

https://doi.org/10.5194/egusphere-2026-4489
Preprint. Discussion started: 13 August 2026

$$e_{s,i} = 611.2 \times \exp\left(\frac{22.46 \times (T - 273.15)}{272.62 + (T - 273.15)}\right) \tag{A1}$$

which agrees with more accurate formulations such as those from Sonntag or Goff-Gratch to within 1% down to 187 K. This formulation has the advantage that it can be differentiated analytically.

The molecular diffusion coefficient of water vapor in $m^2\ s^{-1}$ is calculated as in Picot et al. (2015) following Pruppacher and Klett (2010) as

$$D_v = D_v^0 \left(\frac{p_0}{p}\right)\left(\frac{T}{T_0}\right)^{1.94} \tag{A2}$$

where p is pressure in Pa and the reference diffusivity D_v^0, pressure p_0, and temperature T_0 are 2.11×10^{-5} $m^2\ s^{-1}$,10^5 Pa, 273.15 K respectively.

The latent heat of sublimation L_s is calculated in J m^{-1} following the approximation of Murphy and Koop (2005) as

$$L_s = \left(\frac{1}{M_w}\right)\left(46782.5 + 35.8925T - 0.07414T^2 + 541.5 \exp\left(-\left(\frac{T}{123.75}\right)^2\right)\right) \tag{A3}$$

where M_w is the molar mass of water, taken for the purposes of this equation as 18.015×10^{-3} kg mol^{-1} to be consistent with the source.

When calculating the ice-air interface surface tension σ in as part of the calculation of the critical radius a_k for the Kelvin effect, we follow the same approach as Lewellen (2012) and use the formulation of Hale and Plummer (1974) as

$$\sigma = (141.0 - 0.15T) \times 10^{-3} \tag{A4}$$

in units of J m^{-2}.

To calculate the thermal conductivity of air we follow the polynomial fit suggested by Kannuluik and Carman (1951) converted to W m^{-1} K^{-1} as

$$K = 2.4058 \times 10^{-2}(1 + 0.00317(T - 273.15) - 2.1 \times 10^{-6}(T - 273.15)^2). \tag{A5}$$

https://doi.org/10.5194/egusphere-2026-4489
Preprint. Discussion started: 13 August 2026

The dynamic viscosity of air is calculated in kg m^{-1} s^{-1} following Sutherland (1893) as

$$\mu = 1.458 \times 10^{-6} \left(\frac{T^{1.5}}{T + 110.4} \right). \quad \text{(A6)}$$

Appendix B: Sensitivity of model output to select model parameters

Several model parameters do not have a clear physical basis (Table 1), but may have a strong influence on both the model results and the model speed. We evaluate this by testing how the choice of each parameter influences model runtime, the longwave component of the energy forcing (EF, as a proxy for climate impact which is not sensitive to time of day), the net EF, and peak ice mass. We also evaluate the effect of changes in horizontal eddy diffusivity. Results are shown in Figure B1.

https://doi.org/10.5194/egusphere-2026-4489
Preprint. Discussion started: 13 August 2026

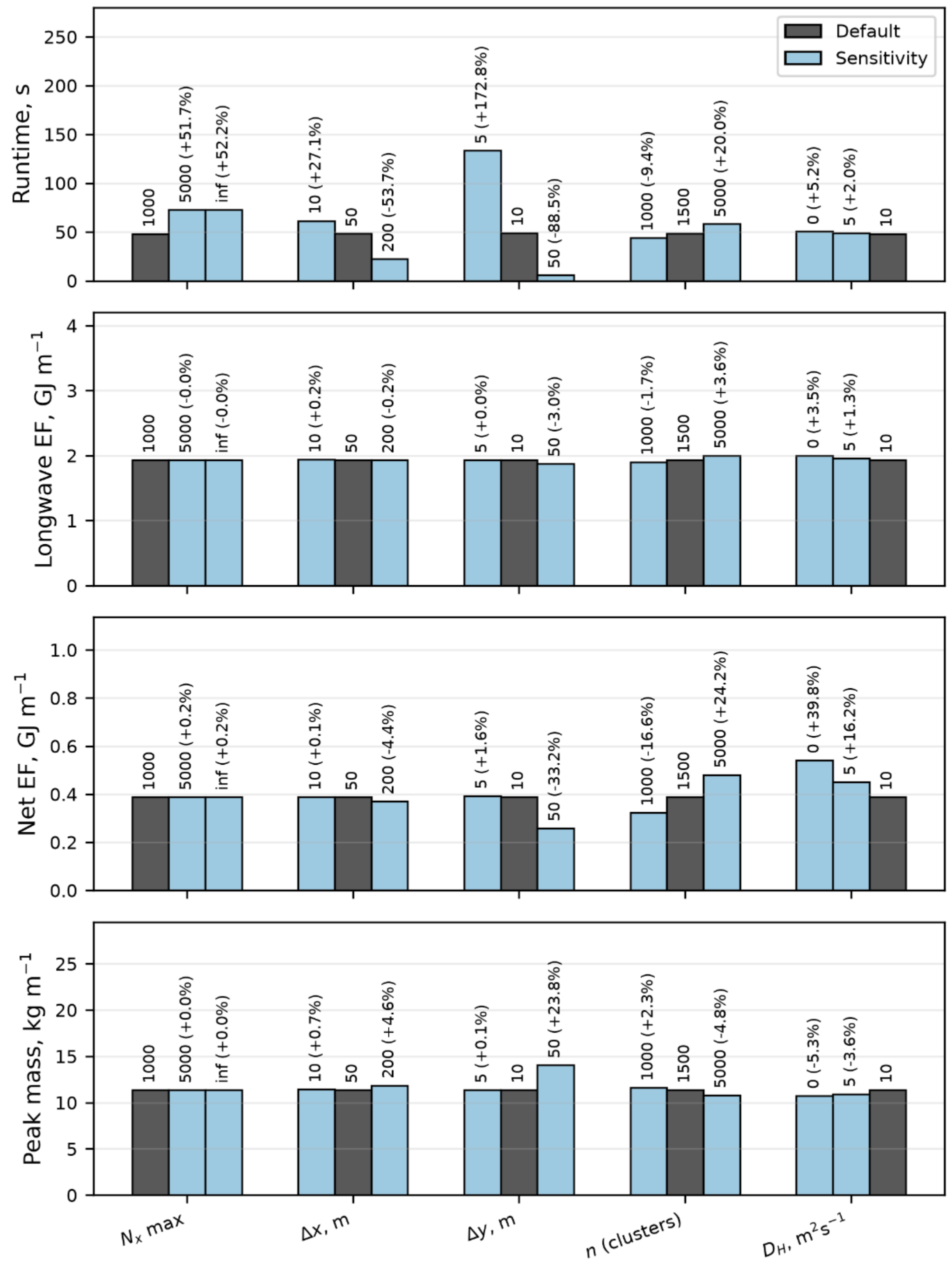

Figure B 1. Sensitivity of model output to parameter settings. Top row: model runtime. Second row: simulated longwave energy forcing (EF). Third row: simulated net EF. Bottom row: peak ice mass. Dark grey bars indicate results using the default value, while pale blue bars indicate a non-default (sensitivity) simulation. The value used for each parameter is listed above the result, along with the percentage difference in the result for non-default simulations. Each bar represents the result averaged across three simulations with all other parameters matching those for the reference simulation (Section 3.1).

https://doi.org/10.5194/egusphere-2026-4489
Preprint. Discussion started: 13 August 2026

All four of the model parameters influence simulation time, but sensitivity of the result varies. Increasing the grid resolution but reducing Δx by five times or Δy by two times increases the model runtime by 27% and 173%, respectively. The effect on model simulation is to change the longwave EF by less than 0.5%, and the peak ice mass by less than 1%. The effect on the net energy forcing is larger due to cancellation between the negative (shortwave) and positive (longwave) components, but still less than 2%. If the resolution is instead decreased (i.e. increasing Δx or Δy by a factor of four or five respectively) then the net EF falls by 4.4% and 33% respectively, but the model runtime also falls by 54% and 89% respectively. This indicates that the current model resolution provides robust results, but could potentially be relaxed somewhat to improve runtimes. Increasing the maximum number of columns (N_x max) from 1,000 to 5,000 increases the simulation time by 52% but causes the net EF to change by 0.2%. This is equivalent to holding the horizontal grid resolution constant at its initial value, as demonstrated by setting N_x max to infinity, and indicates that the automated grid coarsening approach (Section 2.2.9) improves model performance without compromising on accuracy.

The optimal choice for the number of clusters is less clear. Reducing the number from 1500 to 1000 reduces runtime by 9.4%, but also causes the net EF to fall by 17%. Similarly, increasing the count to 5000 increases runtime by 20% and EF by 24%. However, changes in both the longwave EF and peak ice mass are less than 5%. This reflects the fact that the longwave and shortwave EF move in opposite directions with a change in the cluster count. It is likely that this is due to the simplifications used by CLAMP to convert the contrail into a layer for processing by the radiative forcing calculation.

Finally, we consider the effect of horizontal eddy diffusivity. Although technically a meteorological rather than model parameter, we assume in CLAMP that this can be safely set to a representative value rather than being determined based on local meteorology. Reducing the simulated value from 10 to 5 m^2s^{-1} decreases the peak ice mass by 3.6%, and increases the EF by 16%. This relative lack of sensitivity reflects the controlling influence of shear and crystal settling on contrail development, rather than diffusion.

Code availability

The fallstreak package v0.1.1, which includes CLAMP v1.0 as used in this study, can be found at https://doi.org/10.5281/zenodo.21572624 (Eastham and Abbasi, 2026a). Dependencies and installation instructions are provided therein. The most recent version of CLAMP can be downloaded as part of the fallstreak package from https://github.com/ICL-AEIS/fallstreak.

Data availability

All simulation output data are available at https://doi.org/10.5281/zenodo.21568320 (Eastham and Abbasi, 2026b) in the form of NumPy compressed data files. Each data file can be read using NumPy or loaded into a CLAMP simulation using the code version described in the Code Availability section.

Author contributions

SDE conceptualized and implemented the base CLAMP model, carried out all simulations, and prepared the manuscript with contributions from all authors. HRA optimized the model and developed the block assignment algorithm. MEJS, TA, and ZE refined the model scope and helped with model optimization and physics.

Competing interests

The authors declare that they have no conflicts of interest.

Acknowledgements

This work is partially supported by a gift from Breakthrough Energy. The authors would like to thank Dr. Bernd Kärcher, Dr. Kevin Wolf, Prof. Nicolas Bellouin, Dr. Caleb Akhtar Martínez, Dr. Annemarie Lottermoser, and Dr. Simon Unterstrasser for valuable discussion during the design and testing of CLAMP. All simulations are performed using the Imperial College London Department of Aeronautics high performance computing cluster, and verified as reproducible using the Imperial College London CX3 Phase 2 high performance computing facility.

References

Akhtar Martínez, C., Eastham, S. D., and Jarrett, J. P.: Zero-dimensional contrail models could underpredict lifetime optical depth, Atmos. Chem. Phys., 25, 12875–12891, 2025.

Bakels, L., Tatsii, D., Tipka, A., Thompson, R., Dütsch, M., Blaschek, M., Seibert, P., Baier, K., Bucci, S., Cassiani, M., Eckhardt, S., Groot Zwaaftink, C., Henne, S., Kaufmann, P., Lechner, V., Maurer, C., Mulder, M. D., Pisso, I., Plach, A., Subramanian, R., Vojta, M., and Stohl, A.: FLEXPART version 11: improved accuracy, efficiency, and flexibility, Geosci. Model Dev., 17, 7595–7627, 2024.

Barber, C. B., Dobkin, D. P., and Huhdanpaa, H.: The quickhull algorithm for convex hulls, ACM Trans. Math. Softw., 22, 469–483, 1996.

Bickel, M., Ponater, M., Bock, L., Burkhardt, U., and Reineke, S.: Estimating the Effective Radiative Forcing of Contrail Cirrus, J. Clim., 33, 1991–2005, 2020.

https://doi.org/10.5194/egusphere-2026-4489
Preprint. Discussion started: 13 August 2026

Bickel, M., Ponater, M., Burkhardt, U., Righi, M., Hendricks, J., and Jöckel, P.: Contrail cirrus climate impact: From radiative forcing to surface temperature change, J. Clim., 38, 1895–1912, 2025.

Bier, A. and Burkhardt, U.: Impact of parametrizing microphysical processes in the jet and vortex phase on contrail cirrus properties and radiative forcing, J. Geophys. Res., 127, https://doi.org/10.1029/2022jd036677, 2022.

Bock, L. and Burkhardt, U.: Reassessing properties and radiative forcing of contrail cirrus using a climate model, J. Geophys. Res Atmos., 121, 9717–9736, 2016.

Bogacki, P. and Shampine, L. F.: A 3(2) pair of Runge - Kutta formulas, Appl. Math. Lett., 2, 321–325, 1989.

Borella, A., Boucher, O., Shine, K. P., Stettler, M., Tanaka, K., Teoh, R., and Bellouin, N.: The importance of an informed choice of CO_2-equivalence metrics for contrail avoidance, Atmos. Chem. Phys., 24, 9401–9417, 2024.

Bräuer, T., Voigt, C., Sauer, D., Kaufmann, S., Hahn, V., Scheibe, M., Schlager, H., Diskin, G. S., Nowak, J. B., DiGangi, J. P., Huber, F., Moore, R. H., and Anderson, B. E.: Airborne measurements of contrail ice properties—dependence on temperature and humidity, Geophys. Res. Lett., 48, https://doi.org/10.1029/2020gl092166, 2021.

Burkhardt, U., Bock, L., and Bier, A.: Mitigating the contrail cirrus climate impact by reducing aircraft soot number emissions, npj Climate and Atmospheric Science, 1, 37, 2018.

Caiazzo, F., Agarwal, A., Speth, R. L., and Barrett, S. R. H.: Impact of biofuels on contrail warming, Environ. Res. Lett., 12, 114013, 2017.

Chen, C.-C. and Gettelman, A.: Simulated radiative forcing from contrails and contrail cirrus, Atmos. Chem. Phys., 13, 12525–12536, 2013.

Connolly, P. J., Emersic, C., and Field, P. R.: A laboratory investigation into the aggregation efficiency of small ice crystals, Atmos. Chem. Phys., 12, 2055–2076, 2012.

Dalcin, L. D., Paz, R. R., Kler, P. A., and Cosimo, A.: Parallel distributed computing using Python, Adv. Water Resour., 34, 1124–1139, 2011.

Driver, O. G., Stettler, M. E., and Gryspeerdt, E.: Factors limiting contrail detection in satellite imagery, Atmospheric Measurement Techniques, 18, 1115–1134, 2025.

Eastham, S. D. and Abbasi, H. R.: ICL-AEIS/fallstreak: Fallstreak v0.1.1 including CLAMP v1.0, Zenodo, https://doi.org/10.5281/ZENODO.21572624, 2026a.

Eastham, S. D. and Abbasi, H. R.: Simulation results for "Rapid simulation of 2-D contrail cross sections through Contrail Layer Approximation using Multi-crystal Particles (CLAMP) v1.0," https://doi.org/10.5281/ZENODO.21568320, 2026b.

Edelsbrunner, H., Kirkpatrick, D., and Seidel, R.: On the shape of a set of points in the plane, IEEE Trans. Inf. Theory, 29, 551–559, 1983.

Emde, C., Buras-Schnell, R., Kylling, A., Mayer, B., Gasteiger, J., Hamann, U., Kylling, J., Richter, B., Pause, C., Dowling, T., and Bugliaro, L.: The libRadtran software package for radiative transfer calculations (version 2.0.1), Geosci. Model Dev., 9, 1647–1672, 2016.

Engberg, Z., Teoh, R., Abbott, T., Dean, T., Stettler, M. E., and Shapiro, M. L.: Forecasting contrail climate forcing for flight planning and air traffic management applications: the CocipGrid model in pycontrails 0.51. 0, Geoscientific Model Development, 18, 253–286, 2025.

https://doi.org/10.5194/egusphere-2026-4489
Preprint. Discussion started: 13 August 2026

Euchenhofer, M. V., Prashanth, P., Parke, S. A., Eastham, S. D., and Waitz, I. A.: Contrail observation limitations using geostationary satellites, Geophys. Res. Lett., 52, e2025GL118386, 2025.

Field, P. R., Heymsfield, J., Bansemer, A., and Twohy, C. H.: Determination of the combined ventilation factor and capacitance for ice crystal aggregates from airborne observations in a tropical anvil cloud, J. Atmos. Sci., 65, 376–391, 2008.

Fritz, T. M., Eastham, S. D., Speth, R. L., and Barrett, S. R. H.: The role of plume-scale processes in long-term impacts of aircraft emissions, Atmos. Chem. Phys., https://doi.org/10.5194/acp-2019-498, 2020.

Frömming, C., Ponater, M., Burkhardt, U., Stenke, A., Pechtl, S., and Sausen, R.: Sensitivity of contrail coverage and contrail radiative forcing to selected key parameters, Atmos. Environ., 45, 1483–1490, 2011.

Geraedts, S., Brand, E., Dean, T. R., Eastham, S., Elkin, C., Engberg, Z., Hager, U., Langmore, I., McCloskey, K., Yue-Hei Ng, J., Platt, J. C., Sankar, T., Sarna, A., Shapiro, M., and Goyal, N.: A scalable system to measure contrail formation on a per-flight basis, Environ. Res. Commun., 6, 015008, 2024.

Gierens, K.: The utility of partial contrail avoidance, Meteorol. Z., https://doi.org/10.1127/metz/1275, 2025.

Grobler, C., Wolfe, P. J., Dasadhikari, K., Dedoussi, I. C., Allroggen, F., Speth, R. L., Eastham, S. D., Agarwal, A., Staples, Sabnis, J., and Barrett, S. R. H.: Marginal Climate and Air Quality Costs of Aviation Emissions, Environ. Res. Lett., 2019.

Hale, B. N. and Plummer, P. L. M.: Molecular model for ice clusters in a supersaturated vapor, J. Chem. Phys., 61, 4012–4019, 1974.

Harris, C. R., Millman, K. J., van der Walt, S. J., Gommers, R., Virtanen, P., Cournapeau, D., Wieser, E., Taylor, J., Berg, S., Smith, N. J., Kern, R., Picus, M., Hoyer, S., van Kerkwijk, M. H., Brett, M., Haldane, A., Del Río, J. F., Wiebe, M., Peterson, P., Gérard-Marchant, P., Sheppard, K., Reddy, T., Weckesser, W., Abbasi, H., Gohlke, C., and Oliphant, T. E.: Array programming with NumPy, Nature, 585, 357–362, 2020.

Heymsfield, A. J. and Westbrook, C. D.: Advances in the estimation of ice particle fall speeds using laboratory and field measurements, J. Atmos. Sci., 67, 2469–2482, 2010.

Hofer, S. and Gierens, K.: Synoptic and microphysical lifetime constraints for contrails, Atmos. Chem. Phys., https://doi.org/10.5194/acp-25-9235-2025, 2025.

Holton, James R.; Hakim, Gregory J: An introduction to dynamic meteorology, Elsevier S & T, 552 pp., 2012.

Kannuluik, W. G. and Carman, E. H.: The temperature dependence of the thermal conductivity of air, Aust. J. Sci. Res. Ser. A: Phys. Sci., 4, 305–314, 1951.

Kärcher, B.: Formation and radiative forcing of contrail cirrus, Nat. Commun., 9, 1824, 2018.

Kärcher, B. and Corcos, M.: On the lifetimes of persistent contrails and contrail cirrus, J. Geophys. Res Atmos., 130, https://doi.org/10.1029/2025jd044488, 2025.

Kärcher, B. and Podglajen, A.: A stochastic representation of temperature fluctuations induced by mesoscale gravity waves, J. Geophys. Res. D: Atmos., 124, 11506–11529, 2023.

Kärcher, B., Jensen, E. J., Pokrifka, G. F., and Harrington, J. Y.: Ice supersaturation variability in cirrus clouds: Role of vertical wind speeds and deposition coefficients, J. Geophys. Res., 128, https://doi.org/10.1029/2023jd039324, 2023.

Konopka, P.: Analytical Gaussian Solutions for Anisotropie Diffusion in a Linear Shear Flow, J. Non-Equilib. Thermodyn., 20, 73, 1995.

https://doi.org/10.5194/egusphere-2026-4489
Preprint. Discussion started: 13 August 2026

Lee, D. S., Fahey, D. W., Skowron, A., Allen, M. R., Burkhardt, U., Chen, Q., Doherty, S. J., Freeman, S., Forster, P. M., Fuglestvedt, J., Gettelman, A., De León, R. R., Lim, L. L., Lund, M. T., Millar, R. J., Owen, B., Penner, J. E., Pitari, G., Prather, M. J., Sausen, R., and Wilcox, L. J.: The contribution of global aviation to anthropogenic climate forcing for 2000 to 2018, Atmos. Environ., 117834, 2021.

Lewellen, D., Meza, O., and Huebsch, W.: Persistent contrails and contrail cirrus. Part I: Large-eddy simulations from inception to demise, Journal of the Atmospheric Sciences, 71, 4399–4419, 2014.

Lewellen, D. C.: Analytic solutions for evolving size distributions of spherical crystals or droplets undergoing diffusional growth in different regimes, J. Atmos. Sci., 69, 417–434, 2012.

Lewellen, D. C.: Persistent Contrails and Contrail Cirrus. Part II: Full Lifetime Behavior, J. Atmos. Sci., 71, 4420–4438, 2014.

Li, Y., Mahnke, C., Rohs, S., Bundke, U., Spelten, N., Dekoutsidis, G., Groß, S., Voigt, C., Schumann, U., Petzold, A., and Krämer, M.: Upper-tropospheric slightly ice-subsaturated regions: frequency of occurrence and statistical evidence for the appearance of contrail cirrus, Atmos. Chem. Phys., 23, 2251–2271, 2023.

Lohmann, U., Luond, F., and Mahrt, F.: An introduction to clouds: From the microscale to climate, Cambridge University Press, Cambridge, England, 399 pp., 2016.

Lottermoser, A. and Unterstrasser, S.: High-resolution modeling of early contrail evolution from hydrogen-powered aircraft, Atmos. Chem. Phys., 25, 7903–7924, 2025.

Lottermoser, A. and Unterstrasser, S.: Modeling the impact of alternative fuels and hydrogen propulsion on contrail-cirrus: A parameter study, J. Geophys. Res Atmos., 131, e2025JD044604, 2026.

Low, J., Teoh, R., Ponsonby, J., Gryspeerdt, E., Shapiro, M., and Stettler, M. E.: Ground-based contrail observations: comparisons with reanalysis weather data and contrail model simulations, Atmospheric Measurement Techniques, 18, 37–56, 2025.

Märkl, R. S., Voigt, C., Sauer, D., Dischl, R. K., Kaufmann, S., Harlaß, T., and Le Clercq P.: Powering aircraft with 100% sustainable aviation fuel reduces ice crystals in contrails, Atmospheric Chemistry and Physics, 24, 3813–3837, 2024.

Martin Frias, A., Shapiro, M., Engberg, Z., Zopp, R., Soler, M., and Stettler, M. E. J.: Feasibility of contrail avoidance in a commercial flight planning system: an operational analysis, Environ. Res. Infrastruct. Sustain., 4, 015013, 2024.

Murphy, D. M. and Koop, T.: Review of the vapour pressures of ice and supercooled water for atmospheric applications, Q. J. R. Meteorol. Soc., 131, 1539–1565, 2005.

Myhre, G., Kvalevåg, M., Rädel, G., Cook, J., Shine, K. P., Clark, H., Karcher, F., Markowicz, K., Kardas, A., Wolkenberg, P., Balkanski, Y., Ponater, M., Forster, P., Rap, A., Leon, R., and Rodriguez: Intercomparison of radiative forcing calculations of stratospheric water vapour and contrails, metz, 18, 585–596, 2009.

Nelson, J. and Knight, C.: Snow crystal habit changes explained by layer nucleation, J. Atmos. Sci., 55, 1452–1465, 1998.

Nie, J. and Sobel, A. H.: Modeling the interaction between quasigeostrophic vertical motion and convection in a single column, J. Atmos. Sci., 73, 1101–1117, 2016.

Paoli, R., Thouron, O., Cariolle, D., García, M., and Escobar, J.: Three-dimensional large-eddy simulations of the early phase of contrail-to-cirrus transition: effects of atmospheric turbulence and radiative transfer, Meteorol. Z., 26, 597–620, 2017.

https://doi.org/10.5194/egusphere-2026-4489
Preprint. Discussion started: 13 August 2026

Picot, J., Paoli, R., Thouron, O., and Cariolle, D.: Large-eddy simulation of contrail evolution in the vortex phase and its interaction with atmospheric turbulence, Atmos. Chem. Phys., 15, 7369–7389, 2015.

Ponsonby, J., Teoh, R., Kärcher, B., and Stettler, M. E. J.: An updated microphysical model for particle activation in contrails: the role of volatile plume particles, Atmos. Chem. Phys., 25, 18617–18637, 2025.

Pruppacher, H. R. and Klett, J. D.: Microphysics of clouds and precipitation, 2nd ed., Springer Science+Business Media, 975 pp., https://doi.org/10.1007/978-0-306-48100-0, 2010.

Rubin-Zuzic, M., Bugliaro, L., Marsing, A., Wang, Z., Voigt, C., Simson, C., Kaiser, S., and Ziegler, P.: Reduced contrail radiative effect for fleets with low soot and water vapour emissions, Atmos. Environ. X, 27, 100353, 2025.

Schumann, U.: Influence of propulsion efficiency on contrail formation, Aerosp. Sci. Technol., 4, 391–401, 2000.

Schumann, U.: A contrail cirrus prediction model, Geoscientific Model Development, 5, 543–580, 2012.

Schumann, U., Baumann, R., Baumgardner, D., Bedka, S. T., Duda, D. P., Freudenthaler, V., Gayet, J.-F., Heymsfield, A. J., Minnis, P., Quante, M., Raschke, E., Schlager, H., Vázquez-Navarro, M., Voigt, C., and Wang, Z.: Properties of individual contrails: a compilation of observations and some comparisons, Atmos. Chem. Phys., 17, 403–438, 2017.

Smith, J. R., Grobler, C., Hodgson, P. J., Mukhopadhaya, J., Shapiro, M. L., Mirolo, M., Stettler, M. E. J., Eastham, S. D., and Barrett, S. R. H.: The climate opportunities and risks of contrail avoidance, Nat. Commun., 1–12, 2026.

Sobel, A. H., Nilsson, J., and Polvani, L. M.: The weak temperature gradient approximation and balanced tropical moisture waves, J. Atmos. Sci., 58, 3650–3665, 2001.

Spichtinger, P. and Gierens, K. M.: Modelling of cirrus clouds – Part 1a: Model description and validation, Atmos. Chem. Phys., 9, 685–706, 2009.

Sutherland, W.: LII. The viscosity of gases and molecular force, Lond. Edinb. Dublin Philos. Mag. J. Sci., 36, 507–531, 1893.

Teoh, R., Schumann, U., Majumdar, A., and Stettler, M. E. J.: Mitigating the Climate Forcing of Aircraft Contrails by Small-Scale Diversions and Technology Adoption, Environ. Sci. Technol., 54, 2941–2950, 2020.

Teoh, R., Schumann, U., Gryspeerdt, E., Shapiro, M., Molloy, J., Koudis, G., Voigt, C., and Stettler, M. E. J.: Aviation contrail climate effects in the North Atlantic from 2016 to 2021, Atmos. Chem. Phys., 22, 10919–10935, 2022a.

Teoh, R., Schumann, U., Voigt, C., Schripp, T., Shapiro, M., Engberg, Z., Molloy, J., Koudis, G., and Stettler, M. E. J.: Targeted Use of Sustainable Aviation Fuel to Maximize Climate Benefits, Environ. Sci. Technol., https://doi.org/10.1021/acs.est.2c05781, 2022b.

Teoh, R., Engberg, Z., Schumann, U., Voigt, C., Shapiro, M., Rohs, S., and Stettler, M. E.: Global aviation contrail climate effects from 2019 to 2021, Atmospheric Chemistry and Physics, 24, 6071–6093, 2024a.

Teoh, R., Engberg, Z., Shapiro, M., Dray, L., and Stettler, M. E. J.: The high-resolution Global Aviation emissions Inventory based on ADS-B (GAIA) for 2019–2021, Atmos. Chem. Phys., 24, 725–744, 2024b.

Ueda, H., Fukui, T., Kajino, M., Horiguchi, M., Hashiguchi, H., and Fukao, S.: Eddy diffusivities for momentum and heat in the upper troposphere and lower stratosphere measured by MU radar and RASS, and a comparison of turbulence model predictions, J. Atmos. Sci., 69, 323–337, 2012.

https://doi.org/10.5194/egusphere-2026-4489
Preprint. Discussion started: 13 August 2026

Unterstrasser, S.: Large-eddy simulation study of contrail microphysics and geometry during the vortex phase and consequences on contrail-to-cirrus transition, J. Geophys. Res. D: Atmos., 119, 7537–7555, 2014.

Unterstrasser, S.: Properties of young contrails – a parametrisation based on large-eddy simulations, Atmos. Chem. Phys., 16, 2059–2082, 2016.

Unterstrasser, S. and Gierens, K.: Numerical simulations of contrail-to-cirrus transition – Part 1: An extensive parametric study, Atmos. Chem. Phys., 10, 2017–2036, 2010a.

Unterstrasser, S. and Gierens, K.: Numerical simulations of contrail-to-cirrus transition – Part 2: Impact of initial ice crystal number, radiation, stratification, secondary nucleation and layer depth, Atmos. Chem. Phys., 10, 2037–2051, 2010b.

Unterstrasser, S. and Sölch, I.: Study of contrail microphysics in the vortex phase with a Lagrangian particle tracking model, Atmos. Chem. Phys., 10, 10003–10015, 2010.

Unterstrasser, S. and Sölch, I.: Optimisation of the simulation particle number in a Lagrangian ice microphysical model, Geosci. Model Dev., 7, 695–709, 2014.

Unterstraßer, S., Gierens, K., Sölch, I., and Lainer, M.: Numerical simulations of homogeneously nucleated natural cirrus and contrail-cirrus. Part 1: How different are they?, Meteorol. Z., 26, 621–642, 2017.

USDOE Office of Science (SC), Advanced Scientific Computing Research (ASCR), Balay, S., Argonne National Laboratory (ANL), Argonne, IL (United States), Abhyankar, S., Adams, M., Brown, J., Brune, P., Buschelman, K., Constantinescu, E., Dalcin, L., Benson, S., Dener, A., Eijkhout, V., Faibussowitsch, J., Gropp, W., Hapla, V., Isaac, T., Jolivet, P., Karpeev, D., Kaushik, D., Knepley, M., Kong, F., Kruger, S., May, D., McInnes, L., Mills, R., Mitchell, L., Munson, T., Roman, J., Rupp, K., Sanan, P., Sarich, J., Smith, B., Suh, H., Zampini, S., Zhang, H., and Zhang, J.: PETSc/TAO Users Manual Revision 3.24, Argonne National Laboratory (ANL), Argonne, IL (United States), https://doi.org/10.2172/2998643, 2025.

Verma, P. and Burkhardt, U.: Contrail formation within cirrus: ICON-LEM simulations of the impact of cirrus cloud properties on contrail formation, Atmos. Chem. Phys., https://doi.org/10.5194/acp-22-8819-2022, 2022.

Virtanen, P., Gommers, R., Oliphant, T. E., Haberland, M., Reddy, T., Cournapeau, D., Burovski, E., Peterson, P., Weckesser, W., Bright, J., van der Walt, S. J., Brett, M., Wilson, J., Millman, K. J., Mayorov, N., Nelson, A. R. J., Jones, E., Kern, R., Larson, E., Carey, C. J., Polat, İ., Feng, Y., Moore, E. W., VanderPlas, J., Laxalde, D., Perktold, J., Cimrman, R., Henriksen, I., Quintero, E. A., Harris, C. R., Archibald, A. M., Ribeiro, A. H., Pedregosa, F., van Mulbregt, P., and SciPy 1.0 Contributors: SciPy 1.0: fundamental algorithms for scientific computing in Python, Nat. Methods, 17, 261–272, 2020.

Voigt, C., Märkl, R., Sauer, D., Dischl, R., Renard, C., Seeliger, K., Yu, F., Kaufmann, S., Bräuer, T., Jurkat-Witschas, T., Le Chenadec, G., Moreau, J., Requena-Esteban, E., Bonne, N., Vals, M., Roche, A., Zelina, J., Dörnbrack, A., Eirenschmalz, L., Heckl, C., Horst, E., Lichtenstern, M., Marsing, A., Neumann, G., Roiger, A., Scheibe, M., Stock, P., Giez, A., Eckel, G., and Le Clercq, P.: Substantial aircraft contrail formation at low soot emission levels, Nature, 652, 112–118, 2026.

Wolf, K., Bellouin, N., and Boucher, O.: Sensitivity of cirrus and contrail radiative effect on cloud microphysical and environmental parameters, Atmos. Chem. Phys., 23, 14003–14037, 2023.